Development of Polymer Nanosheet for Wound Dressing Materials

創傷被覆材としての 高分子ナノシートの開発

A Thesis
Presented to
Waseda University

July 2013

Akihiro SAITO

齋藤　晃広

Development of Polymer Nanosheet for Wound Dressing Materials

創傷被覆材としての 高分子ナノシートの開発

A Thesis
Presented to
Waseda University

Waseda University
Graduate School of Advanced Science and Engineering
Major in Life Science and Medical Bioscience,
Research on Biomolecular-Assembly

July 2013

Akihiro SAITO

齋藤　晃広

Promoter: Prof. Dr. Shinji Takeoka
Referees: Prof. Dr. Yasuo Ikeda
Prof. Nobuhito Goda

Preface

Recently, technology of science has become increasingly important in the medical field. For Example, in the field of “wound dressing material”, medical knowledge is obviously needed for application, science knowledge is required the design that can demonstrate the most efficient and effective of the material. The conventional wound dressing material has a problem that management of the wound-care (or infection) process is difficult to monitor visually through the overlaid dressings because none of these materials is transparent. Moreover, The materials doesn’t have enough adhesiveness. Therefore, the new type of wound dressing material that can play on-demand treatment. has expected.

Against this background, the author focused on polymer ultra-thin film “nanosheet”. Nanosheet has a unique properties owing huge aspect ratio; [i] high flexibility, [ii] high adhesiveness and [iii] high transparency. If the nanosheet made of biocompatible polymer, The nanosheet would be a revolutionary medical material.

This thesis consisted of seven chapters. The first chapter deals with the core principles of nanomaterials science and nanotechnology in the basis of self-assembly. And then, the fundamental aspects of wound dressing material are explained. The second chapter deals with fundamental aspects of nanosheet. The construction method and unique properties are described. In chapter 3-5, the medical applications of nanosheet are described. The concept is “the high transparency self-attached wound dressing material that can cover flat to high curvature surface”. In chapter 3, the standard nanosheet applications is described; the haemostatic material for massive haemorrhage from vena cava. In chapter 4 and 5, the functionalized nanosheet application is described. Fragmented nanosheet that can cover the complex and huge surface is introduced in chapter 4. The fragmented nanosheet apply for partial thickness burn and protective efficiency against bacterial infection. Antimicrobial loaded nanosheet is introduced in chapter 5. The nanosheet apply for full-thickness burn with infection injury. Finally, the conclusion and the future prospects of this thesis are described in chapter 6.

As the medicalapplication of the nanosheet, the author is convincedthat the author convinced that the nanosheet is revolutionary development of wound dressing material that can on-demand wound observation under the surgery and after operation.

Akihiro Saito

Contents

Chapter 1.

Fundamental aspects of soft materials and wound dressing materials

1. Fundamental aspects of soft materials

1.1. Principle of self-assembly

Self-assembly is approach for fabricating novel supramolecular architectures [1]. In nature, there are various self-assembly (e.g. cell architecture composed of lipid molecules, oxygen carrying in blood by hemoglobin, ribosomal proteins and RNA association in ribosomes). Self-assembly involves secondly and/or non-covalent bonds (e.g. hydrogen bonds, electrostatic interactions, hydrophobic effect, van der Waals interactions). They govern the structural conformation of all macromolecules and influence their interaction with other molecules.

Two main types of self-assembly have been identified by Whitesides; static self-assembly and dynamic self-assembly (Table 1.1) [2]. Static self-assembly (S) involves systems that are local equilibrium and do not decrease energy (e.g. molecular crystal). Although the formation of a structure may require energy, once it is formed, it is stable. On the other hand, in dynamic self-assembly (D), the formation of structures or patterns occurs when the system decrease energy (e.g. biological cells). Additionally, they define two further variation of self-assembly; templated self-assembly and biological self-assembly.

Table 1.1 Examples of self-assembly (S: static, D: dynamic, T: template, B: biological) [2]

System	Applications/importance	Type
Atomic, ionic, and molecular crystals	Materials, optoelectronics	S
Phase-separated and ionic layered polymers		S
Self-assembled monolayers (SAMs)	Microfabrication, sensors, nanoelectronics	S, T
Lipid bilayers and black films	Biomembranes, elusions	S
Liquid crystals	Displays	S
Colloidal crystals	Band gap materials, molecular sieves	S
Bubble rafts	Models of crack propagation	S
Macro- and mesoscopic structures (MESA)	Electronic circuits	S or D, T
Fluidic self-assembly	Microfabrication	S, T
"Light matter"		D, T
Oscillating and reaction-diffusion reactions	Biological oscillations	D
Bacterial colonies		D, B

Templated self-assembly (T) is determination of structures due to interactions between the components and regular features in their environment. Biological self-assembly (B) is the variety and complexity of the functions that it produces.

1.2. Soft nanotechnology

Soft nanotechnology is developing technology using of "soft matter", which is included self-assembled polymer, peptide, lipids, proteins, colloids and other organic materials. There are two kind of nanotechnology to fabricate soft matter. First one is top-down approach. Another one is bottom-up approach. The top-down approach uses the nanofabrication methods. For example, photo- or electron beam- patterning and lithography techniques belong to this category. Although 2 and 3D structures are formed using top-down approach, these structures are limited by the inherent two-dimensionality [9]. On the other hand, bottom-up approach uses the self-assembly thorough the molecule by molecule or atom by atom [10]. Bottom-up approach has higher resolution than top-down.

1.3. Ultra thin film preparation methodology

Several methodology of ultra thin film preparation using bottom-up approach have been developed widely such as the Langmuir-Blodgett (LB) method, the self-assembled monolayer (SAM) method and Layer-by-Layer (LbL) method.

In the 1930s, the LB method was developed. The LB method is performed following steps (Fig. 1.1) [11]. First, amphiphilic molecules dissolving in organic solvents are spread onto the water surface. After evaporating the organic solvent, the amphiphilic molecules are trapped on the water surface, and then, they form a monolayer onto substrates. In the same manner, LB method can increase the molecular layers. Additionally, the LB technique is

applied for not only amphiphilic molecules but also various molecules; polymers [12], nanowire [13] and graphite oxide [14].

The SAM method is ordered molecular assemblies based on constituent molecules (Fig. 1.2) [15, 16]. The constituent molecules (referred as ligand or headgroup) have a specific and high affinity for the surface of substrates that are metals, metal oxides, and semiconductors. The general researches of SAM are that alkanethiols as headgroup bind to metal substrates such as gold [17-19], silver [20, 21] and copper [22]. The SAM is suited for nano-scale study because [i] it prepares easy (special equipment is not need), [ii] it forms on various sizes of objects (surface of not only thin films but also nanowires, colloids, and other nanostructures) and [iii] it links nano-structures to macroscopic interfaces.

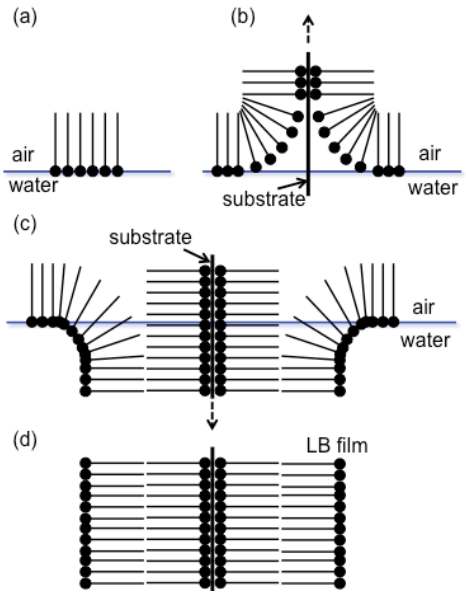

Fig. 1.1 Schematic representation of LB method. (a) amphiphilic molecule is spread at the air-water interface. (b) a substrate is passed through the interface. And then, LB film is fabricated. (c, d) second layer is fabricated by second pass. [12]

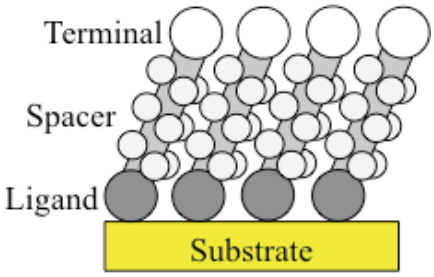

Fig 1.2 Schematic ideal illustration SAM of alkanethiolates supported on a gold surface. [16]

The LbL method is regarded as a versatile bottom-up nanofabrication technique because there are various combinations of multilayer formation and materials (Fig. 1.3) [23]. The general driving force of LbL method is through electrostatic interaction although many kinds of interactions have been used (such as hydrogen bond [24, 25], π–π interaction [26], covalent bond [27] and biospecific interaction [28]) (Fig. 1.3). The materials are not only polymers but also nanomaterials such as nanoparticles [29], carbon nanotube [30] and grapheme [31]. The LbL method can precisely control the nanostructured size and thick by control the layer pairs.

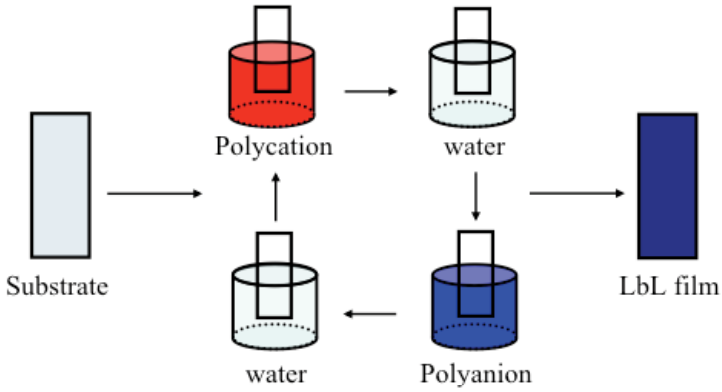

Fig. 1.3 Outline of LbL assembly through electrostatic interaction. [23]

The LbL method is easy to fabricate the functionalized film selecting the appropriate components. For example, Irvine and coworkers develop the DNA vaccine delivery film coated onto microneedle [32]. Additionally, some development procedure of the LbL film is reported. For example, Char and coworkers reported a spin-coating LbL method (Fig. 1.4 (a)) [33]. Compared with conventional dipping method, it takes very short process time. On the other hand, Decher and coworkers proposed spraying procedure (Fig. 1.4 (b)) [34]. The procedure can fabricating the nanostructure onto the 3D object.

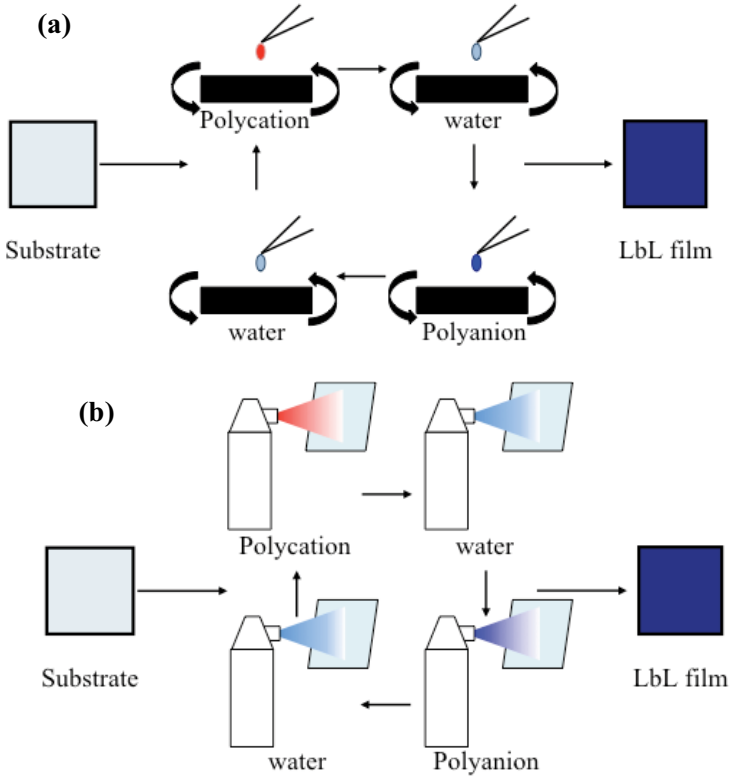

Fig. 1.4 Advanced techniques for LbL method; (a) spin-coating [33] and (b) spraying procedure [34].

2. Fundamental aspects of wound dressing materials

2.1. Wound and its healing process

Wound is “a disruption in the normal anatomic structure continuity and function, resulting from physical, thermal damage or so on” [35, 36].

The wound healing process is a biologically specific that is the general phenomenon of growth and tissue regeneration. The wound healing process are five stages described by Schultz [37]. These are described as [i] haemostasis, [ii] inflammation, [iii] migration, [iv] proliferation, and [v] maturation (or remodeling) phases (Fig. 1.5) [38]. First, bleeding is occurred at the wound site, and then haemostasis and inflammatory are immediately occurred until 1 to 3 days. Haemostasis make a clot to protect the wound site against bacterial infection. Inflammatory involves cellular response. Next, the cell migration is occurred until 3 - 5days. The epithelial cells and fibroblasts move to wound area to heal the damaged and lost tissue. After migration, the proliferation is occurred until 2 weeks after injury. In this phase, granulation, epithelialization and vascularization is active. Finally, each cellular fabricate connective tissue with new epithelium layer. All wound healing processes finish from 1 - 2 months up to 2 years.

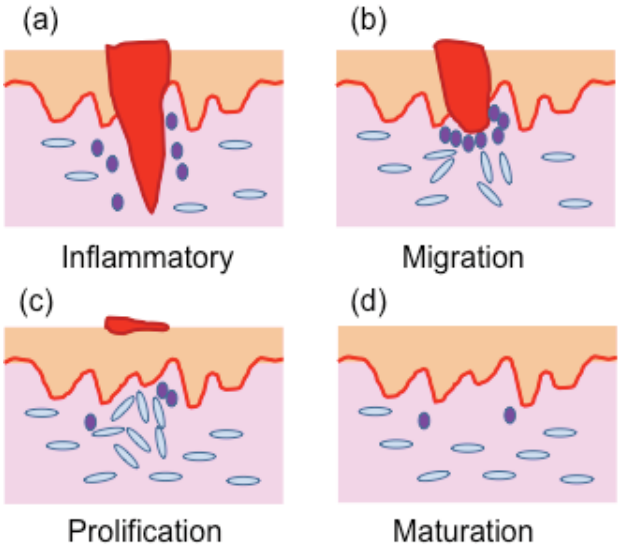

Fig. 1.5 Schematic representation of wound healing process ; (a) haemostasis and infalammatory, (b) migration, (c) proliferation, and (d) maturation phases [38]

2.2. Wound dressing material

In order to heal wound quickly and smoothly as described above, we should select appropriate wound dressing material. There are three main factors that must be considered when choosing a suitable dressing material [36]: [i] controlling infection in the wound; [ii] generating a moist environment for healing; [iii] protection of the wound area from mechanical trauma. Traditionally, cotton gauze has been used as a wound-dressing material that can protect against bacteria. Unfortunately, these dressings adhere to the wound area, causing pain and further tissue damage [39]. Recently, there are many kind of wound dressings, and are classified the materials, such as hydrofiber dressing (e.g. Aquacel®, ConvaTec Co.) [40, 41], hydrocolloids (e.g. Dodder®, ConvaTec Co.) [42], form dressings (e.g. Geben cream®, Tanabe Mitsubishi Pharma Co.) [43]. However, because none of these materials is transparent, management of the wound-care (or infection) process is difficult to monitor visually through the overlaid dressings. Therefore, the new type of wound dressing material that can play on-demand treatment has expected.

References

1) S. Zhang, *Nat. Biotechnol.* **21**, 1171 (2003).

2) G. M. Whitesides, B. Grzybowski, *Science*, **295**, 2418 (2002).

3) J. D. Hartgerink, E. Beniash, S. Stupp, *Science*, **294**, 1684 (2001).

4) N. Ban, P. Nissen, J. Hansen, P. B. Moore, T. A. Steitz, *Science*, **289**, 905 (2000).

5) D. H. Gracias, V. Kavthekar, J. C. Love, K. E. Paul, G. M. Whitesides, *Adv. Mater.*, **14**, 235 (2002).

6) T. D. Clark, J. Tien, D. C. Duffy, K. E. Paul, G. M. Whitesides, *J. Am. Chem. Soc.*, **123**, 7677 (2001).

7) R. F. Ismagilov, D. Rosmarin, D. H. Gracias, A. D.Strook, G. M. Whitesides, *Appl. Phys. Lett.*, **79**, 439 (2001).

8) G. M. Whitesides, R. F. Ismagilov, *Science*, **284**, 89 (1999).

9) R. Shenhar, V. M. Rotello, *Acc. Chem. Res.*, **36**, 549 (2003).

10) J. A. Zasadzinski, R. Viswanathan, L. Madsen, J. Garnaes, D. K. Schwartz, *Science*, **263**, 1726 (1994).

11) I. W. Hamley, *Angew. Chem. Int. Ed.*, **42**, 1692 (2003).

12) N. Reitzel, D. R. Greve, K. Kjaer, P. B. Hows, M. Jayaraman, S. Savoy, R. D. McCullough, J. T. McDevitt, T. J. Bjornholm, *Am. Chem. Soc.*, **122**, 5788 (2000).

13) D. Whang, S. Jin, Y. Wu, C. M. Lieber, *Nano Lett.*, **3**, 1255 (2003)

14) J. C. Laura, K. Franklin, H. Jiaxing, *J. Am. Chem. Soc.*, **131**, 1043 (2009).

15) A. Ulman, *Chem. Rev.*, **96**, 1533 (1996).

16) J. C. Love, L. A. Estroff, J. K. Kriebel, R. G. Nuzzo,, G. M. Whitesides, *Chem. Rev.*, **105**, 1103 (2005).

17) G. E. Poirier, E. D. Pylant, *Science,* **272**, 1145 (1996).

18) L. H. Dubois, R.G. Nuzzo, *Annu. Rev. Phys. Chem.*, **43**, 437 (1992).

19) C. D. Bain, J. Evall, G.M.Whitesides, *J.Am.Chem.Soc.*, **111**, 7155 (1989).

20) M. M.Walczak, C. Chung, S. M. Stole, C. A. Widrig, M. D. Porter, *J. Am. Chem. Soc.*, **113**, 2370 (1991).

21) P. Fenter, P. Eisenberger, J. Li, N. Camillone, S. Bernasek, G. Scoles, T. A. Ramanarayanan, K. S. Liang, *Langmuir*, **7**, 2013 (1991).

22) P. E. Laibinis, G. M. Whitesides, D. L. Allara, Y. T. Tao, A. N. Parikh, R. G. Nuzzo, *J. Am. Chem. Soc.*, **113**, 7152 (1991).

23) K. Ariga, J. P. Hill, Q. Ji, *Phys. Chem. Chem. Phys.*, **9**, 2319 (2007).

24) W. Stockton, M. F. Rubner, *Macromolecules*, **30**, 2717 (1997).

25) H. Lee, R. Mensire, R. E. Cohen, M. F. Rubner, *Macromolecules*, **45**, 347 (2012)

26) T. Tang, J. Qu, K. Mullen, S. E. Webber, *Langmuir*, **22**, 26 (2006)

27) G. K. Such, J. F. Quinn, A. Ouinn, E. Tjipto, F. Caruso, *J. Am. Chem. Soc.*, **128**, 9318 (2006).

28) K. Sato, Y. Imoto, J. Sugama, S. Seki, H. Inoue, T. Odagiri, T.Hoshi, J. Anzai, *Langmuir,* **21**, 797 (2005).

29) S. Yang, Y. Zhang, L. Wang, S. Hong, J. Xu, Y. Chen, C. Li, *Langmuir*, **22**, 338 (2006).

30) A. B. Artyukhin, O. Bakajin, P. Stroeve, A. Noy, *Langmuir*, **20**, 1442 (2004).

31) M. Yanga, Y. Houd, N. A. Kotov, *Nano Today*, **7**, 430 (2012)

32) P. C. DeMuth, Y. Min, B. Huang, J. A. Kramer, A. D. Miller, D. H. Barouch, P. T. Hammond, D. J. Irvine, *Nat Matter*, **12**, 367 (2012)

33) J. Cho, K. Char, J. D. Hong, K. B. Lee, *Adv. Mater.,* **13**, 1076 (2003).

34) A. Izquierdo, S. S. Ono, J. C. Schaaf, G. Decher, *Langmuir*, **21**, 7558 (2005).

35) C. Cochrane, M. G. Rippon, A. Rogers, R. Walmsley, D. Knottenbelt, P. Bowler,

Biomaterials, **20**, 1237 (1999).

36) W. Zhong, M. M. Q. Xing, H. I. Maibach, *Cutaneous Ocular Toxicol.*, **29**, 143 (2010).

37) G. S. Schultz, Molecular regulation of wound healing. In: Bryant RA, editor. Acute and chronic wounds: Nursing management. 2nd edition. St. Louis, MO: Mosby. pp 413–429 (1999).

38) J. S. Boateng, K. H. Matthews, H. N. E. Stevens, G. M. Eccleston, *J. Pharmacol. Sci.*, **97**, 2892 (2008).

39) C. Cochrane, M. G. Rippon, A. Rogers, R. Walmsley, D. Knottenbelt, P. Bowler, *Biomaterials*, **20**, 1237 (1999).

40) A. Burd, C. H. Kwok, S. C. Hung, H. S. Chan, H. Gu, W. K. Lam, *et al.*, *Wound Repair. Regen.*, **15**, 94 (2007).

41) S. A. Jones, P. G. Bowler, M. Walker, D. Parsons, *Wound Repair. Regen.*, **12**, 288 (2004).

42) J. P. Draye, B. Delaey, A. V. Voorde, V. D. Bulcke, B. Reu, E. Schacht, *Biomaterials*, **19,** 1677 (1998).

43) K. Hirose, H. Onishi, M. Sasasatsu, K. Takeshita, K. Kouzuma, K. Isowa, *et al*., *Biol. Pharm. Bull.*, **30**, 2406 (2007).

Chapter 2.

Fundamental aspects of polymer ultra-thin film ” Nanosheet”

1. Fundamental aspects of nanosheet

1.1. Development of polymer ultra-thin film “nanosheet”

As described chapter 1, soft nanotechnology is significantly developed. In particular, polymer ultra-thin film (refereed as nanosheet) which the thickness size is “nm” scale has been studied by many researchers.

In order to apply for bio-applications, we developed LbL nanosheet composed of biocompatible polymer [1, 2]. The nanosheet is fabricated by spin-coating method because the surface is highly smooth (RMS < 5 nm). Moreover, comparing dipping method, spin-coating method can rapidly fabricate the nanosheets. Actually, spin-coating method can easily fabricate the single layer nanosheet (Fig. 2.1) [3]. To decrease the concentration of polymer solution (e.g. 1.0 wt.%), the thickness of resulting film is “nm” scale.

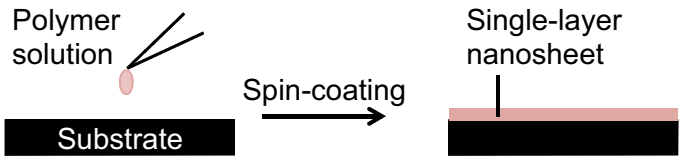

Fig. 2.1 Schematic representation of single-layer nanosheet fabricated by spin-coating method

1.2. Peeling off method of nanosheet

Although the many researchers research about ultra-thin film, most researches are on substrate research. Therefore, in order to obtain a “free-standing” nanosheet in the air, we focused on ‘‘supporting film’’ method [4]. The supporting film consists of water-soluble polymer and thickness is 10 - 20 μm. The function of supporting layer is peeling from the substrate with nanosheet. This method allows the nanosheet detached from substrate and handled easily in the air. As the supporting layer, we selected poly(vinyl alcohol) (PVA). The PVA aqueous solution was casted onto nanosheet and dried completely (Fig. 2.2). The resulting bilayered film was easily peeled from substrate, and then, the only nanosheet can be obtained to dissolve PVA layer by water. Therefore, the nanosheet can be transferred onto

various surfaces. This methodology is suitable for wound dressing materials application.

Fig. 2.2 Schematic representation of supporting film method to peel off the nanosheet from substrate

Another peeling off method is "sacrificial layer" method [1]. Before polymer nanosheet fabricate, PVA ultra-thin layer (~15 nm) is fabricated (Fig. 2.3). When the substrate immersed into water, nanosheet is peeled from substrate and free-standing in water. This method is significantly less amount of PVA than supporting film method although the nanosheet can't free-standing in the air.

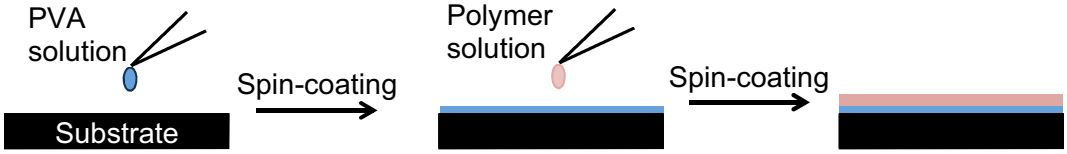

Fig. 2.3 Schematic representation of sacrificial layer method to peel off the nanosheet from substrate in water.

1.3. Construction of biocompatible LbL nanosheet

Although there are various combinations of fabricating LbL nanosheet, we focused on biocompatible LbL nanosheet [1, 2, 5]. Here, the construction method of LbL nanosheet composed of chitosan and Na alginate is explained. Chitosan derived from crab is polycation, on the other hand Na alginate derived from sea weeds is polyanion. The LbL nanosheets were prepared using the following steps (Fig. 2.4): 1) dropping 1 mL of Chitosan (1 mg/mL, 1% (v/v) acetic acid) or Na alginate (1 mg/mL) solution onto a SiO_2 substrate and rotating at 4,500 rpm (revolutions per minute) for 15-20 seconds repeatedly; 2) drying the surface by N_2 flow; 3) casting of the supporting layer from a 10% PVA aqueous solution for over 12 hours and drying; 4) peeling the film (polysaccharide nanosheet with the PVA) from the SiO_2 substrate. The resulting nanosheet was approximately 75 nm thick measured by Atomic force microscope (AFM). The same nanosheet was used at chapter 4.

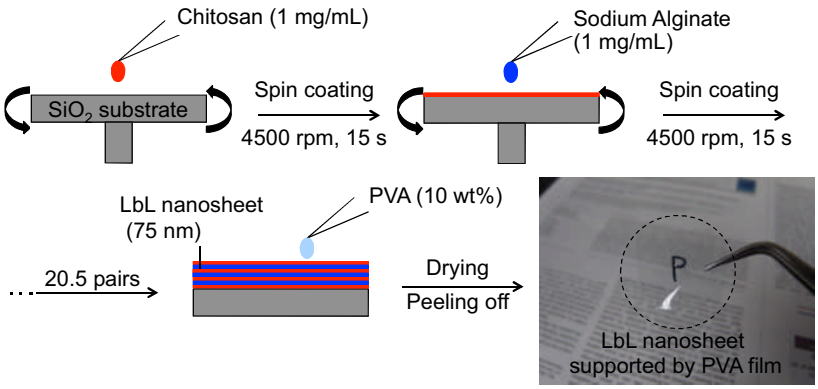

Fig. 2.4 Schematic representation of free-standing LbL nanosheet.

1.4. Construction of single layer nanosheet

As described Fig. 2.1, the single layer nanosheet was fabricated by spin-coating method. We previously reported some polymers that can construct the nanosheet. The component is poly(lactic acid) (PLA) that is biocompatible and biodegradable polymer [6]. PLA is used as degradable sutures, bone screws, pins, and plates in the medical field [7, 8].

2. Physical characteristics of nanosheet

2.1. Mechanical property

The bulge test is used for evaluation of the mechanical strength for the nanosheets (Fig. 2.5). The bulge test has been used for the evaluation of the mechanical strength of ultra-thin films [9]. The stress-strain curve is calculated by eq. 2.1 to measure the nanosheet deflection.

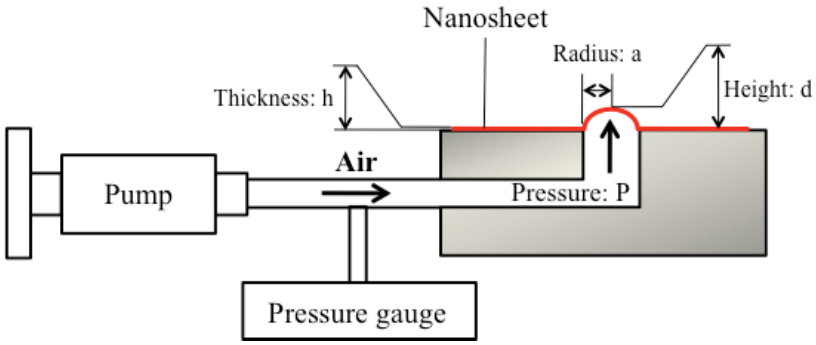

Fig. 2.5 Schematic representation of bulge test

$$\text{Strain: } \sigma = (P \times a^2)/(4 \times h \times d)$$
$$\text{Stress: } \varepsilon = (2 \times d^2)/(3 \times a^2) \qquad \text{(eq. 2.1)}$$
$$\text{Elastic modulus: } E = \sigma / \varepsilon$$

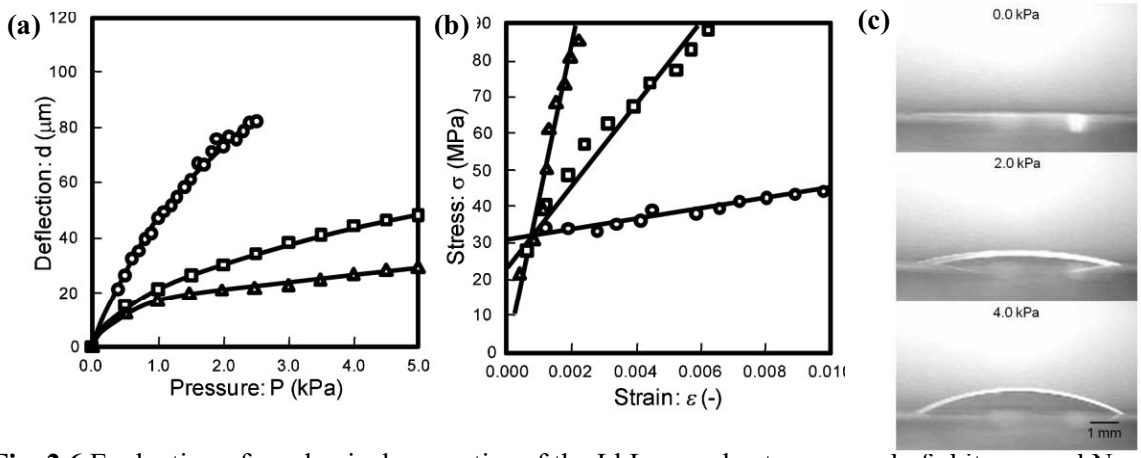

Fig. 2.6 Evaluation of mechanical properties of the LbL nanosheet composed of chitosan and Na alginate. (a) Relationship of pressure-deflection (b) Relationship of stress-strain calculated by eq.2.1 (Each thickness of LbL nanosheet is ○: 35 nm, △: 75 nm and □: 114 nm) (c) Macroscopic cross-sectional images of the 75 nm of LbL nanosheet (adapted with permission from ref. 10 Copyright Wiley 2009).

The results of LbL nanosheet composed of chitosan and Na alginate are shown in Fig. 2.6 [10]. The elastic modulus calculated by stress strain curve was decreased with decreasing the nanosheet thickness. The result indicated that the nanosheet become softer to decrease the thickness. In general, ultra-thin polymer films show glass-transition temperatures lower than the bulk films [11]. Therefore, the nanosheets have low elastic moduli. The similar result is reported about different types of nanosheet [6].

2.2. Adhesive property

In order to evaluate the physical adhesive property of nanosheet, the micro scratch test is utilized. The procedure in brief is as follows; a diamond tip at a radius of curvature of 100 μm is continuously and vertically loaded at a rate of 10 mN/min, and horizontally scratched the nanosheet. The signal of frictional vibration just after breaking of the PLLA nanosheet is detected as a critical load.

The results of LbL nanosheet composed of chitosan and Na alginate are shown in Fig. 2.7 [10]. Adhesive strength of LbL nanosheets did not change before and after detachment

from substrate. Interestingly, in the case of thickness of LbL nanosheet was under 200nm, the critical load of the LbL nanosheets was drastically increased (Fig. 2.7 (a)). Furthermore, the defected shape was different under and over 200 nm thick (Fig. 2.7 (b)). These results indicated that the elasticity of nanosheet would be different for thicknesses above and below 200 nm. These results are followed mechanical property test. The result of adhesive property is similar to PLA nanosheet. Therefore, these flexibility and adhesive strength is unique properties of polymer nanosheet. Moreover, the nanosheets are high transparent material owing to their thickness. These properties are suitable for wound dressing materials for not only surgical but also traumatic applications. The concepts of nanosheet treatment are [i] self-adhesive to injured site without other chemical glue, [ii] covering not only flat surface but also high curvature or complex surfaces, and [iii] on-demand treatment under operation as well as follow-up treatment.

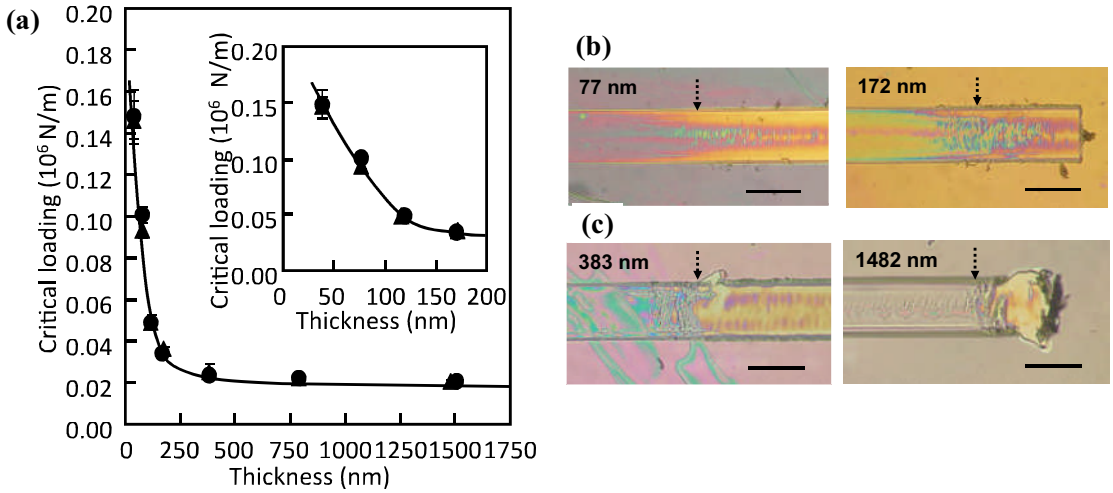

Fig. 2.7 Evaluation of adhesive properties of the LbL nanosheet (s) Relationship between thickness and critical loading that means adhesive strength (●: before freestanding, ▲: after freestanding). (b, c) LbL nanosheet defected images after micro scratch test. In the case of under 200 nm thick, the defect shape is drawn trail. In contrast, in the case of over 200 nm thick, the defect shape is cut trail. [10] (adapted with permission from ref. 10 Copyright Wiley 2009).

References

44) T. Fujie, Y. Okamura, S. Takeoka, *Adv. Mater.*, 19, 3549 (2007).

45) T. Fujie, S. Furutate, D. Niwa, S. Takeoka, *Soft Matter*, **6**, 4672 (2010).

46) Y. Okamura, K. Kabata, M. Kinoshita, D. Saitoh, S. Takeoka, *Adv. Mater.*, **21**, 4388 (2009).

47) A. D. Stroock, R. S. Kane, M. Weck, S. J. Metallo, G. M. Whitesides, *Langmuir*, **19**, 2466 (2003).

48) T. Fujie, H. Haniuda, S. Takeoka, *J. Mater. Chem.*, **21**, 9112 (2011)

49) Y. Okamura, K. Kabata, M. Kinoshita, D. Saitoh, S. Takeoka, *Adv. Mater.*, **21**, 4388 (2009).

50) J. Conn, R. Oysasu, M. Welsh, J. Beal, *Am. J. Surg.*, **128**, 19 (1974).

51) D. A. McGuire, F. A. Barber, B. F. Elrod, L. E. Paulos, *Arthroscopy*, **15**, 463 (1999).

52) S. Markutsya, C. Jiang, Y. Pikus, V. V. Tsukruk, *Adv. Funct. Mater.,* **15**, 771 (2005)

53) T. Fujie, N. Matsutani, M. Kinoshita, Y. Okamura, A. Saito, S. Takeoka, *Adv. Funct. Mater.*, **19**, 2560 (2009)

54) J. A. Forrest, K. Dalnoki-Veress, J. R. Stevens, J. R. Dutcher, *Phys. Rev. Lett.*, **77**, 2002 (1996)

Chapter 3.

Haemostatic efficiency of nanosheet in rabbit IVC incised model

1. Introduction

Massive hemorrhage from injured large blood vessels causes morbidity and mortality in trauma patients. Many clinical reports have demonstrated that major venous injuries are usually accompanied with other organ injuries, are sometimes lethal, and require highly trained individuals to perform their repair [1-4]. Although suturing repair is usually performed when a large vessel is injured, suture of venous wall injuries is sometimes technically difficult because of their structural fragility. Patients receiving lateral venorrhaphy following suturing repair occasionally develop complications such as chronic severe stenosis or thrombotic occlusion of the IVC with lower extremity edema [5-7]. It is known that ligation of large veins is a limited option for damage control surgery [8, 9], and this is especially true for perforated bleeding from proximal central veins such as the superior vena cava (SVC), inferior vena cava (IVC) and pulmonary veins. Conventional hemostatic materials such as collagen fleece and polymeric mesh have a limited ability to stop the bleeding from large vessels because these materials are thick (over 1 mm) and thus do not adhere well. Furthermore, these materials induce inflammation of the injury site in order to trigger the healing process and such inflammation sometimes influences post-surgical adhesion.

In this chapter, we applied the nanosheet for venous haemostatic material. The nanosheet is covered on high curvature site such as vessels owing to their flexibility. Houwever, if the haemostasis is not succeeded completely, the small amount of haemorrhage (oozing) will be confirmed owing to their transparency. In this case, we propose “multi-overlapping therapy” for large venous bleeding sites such as IVC to improve the mechanical durability (Fig.4.1). A nanosheet is adhered to the injured site by physical adsorption, on which another nanosheet is overlapped until the bleeding stops. This methodology not only increases the durability of the single nanosheet without losing the

adhesive force, but also minimizes the absolute mass of the polymers used inside the body. We investigated the efficacy of multi-overlapping nanosheets for sealing and stopping hemorrhage of large venous injuries using an *in vitro* silicon tube model and an *in vivo* IVC injury rabbit model.

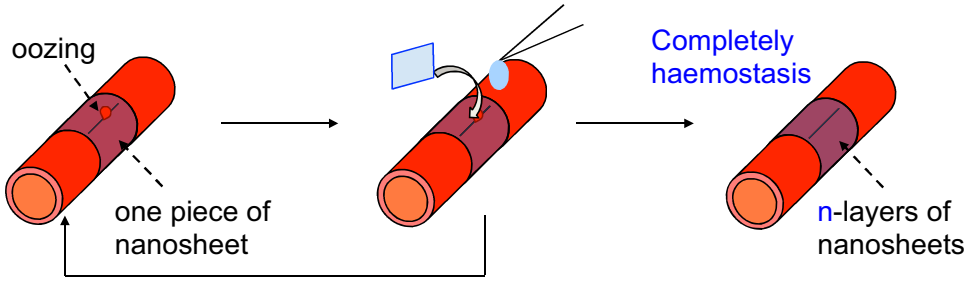

Fig. 4.1 Conceptual image of "multi-overlapping therapy".

2. Construction of free-standing LbL nanosheet

Spin-coating-assisted LbL (SA-LbL) assembly was performed by following the method described in our previous report [10]. Briefly, the nanosheets were prepared using the following steps (Chapter 2): 1) dropping 1 mL of Chitosan (1 mg/mL, 1% (v/v) acetic acid) or Na alginate (1 mg/mL) solution onto a SiO2 substrate and rotating at 4,500 rpm (revolutions per minute) for 15-20 seconds repeatedly; 2) drying the surface by N_2 flow; 3) casting of the supporting layer from a 10% PVA aqueous solution for over 12 hours and drying; 4) peeling the film (polysaccharide nanosheet with the PVA) from the SiO_2 substrate (Fig. 1B). The resulting nanosheet was approximately 75 nm thick measured by AFM.

3. Evaluation of hydrostatic durability and physiological stability

3.1. Hydrostatic durability test

The ability to resist hydrostatic pressure as a measure of mechanical durability of the nanosheet was evaluated by means of bursting pressure using a silicon tube model

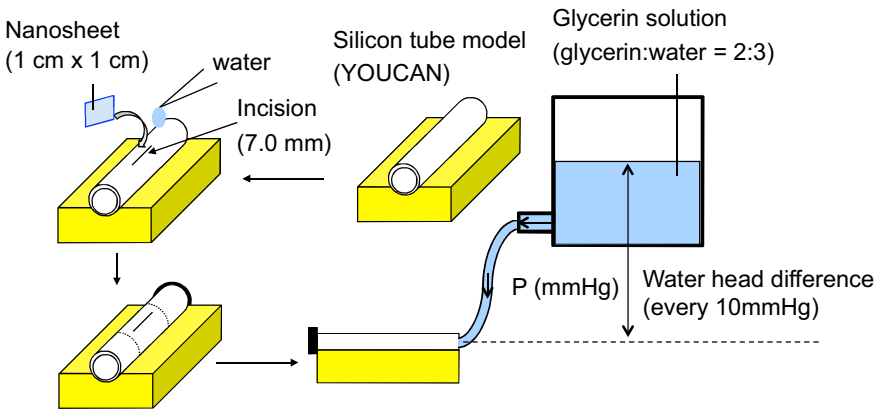

Fig. 4.2 Schematic representation of hydrostatic durability test.

(YOUCAN, EBM Co., Tokyo, Japan) [11] (Fig. 4.2, 4.3). YOUCAN is made of silicon rubber and its elasticity was controlled by the ratio of compounded silicon oil. We adjusted the size and Young's modulus of the silicon tube to that of mammalian vessels, thereby simulating rabbit IVC (inner diameter: 4 mm, outer diameter: 5 mm, Young's modulus: 0.113 MPa). The silicon tube was longitudinally incised 7 mm at the center of the tube. The nanosheet with PVA was transferred onto the incision. Upon placement, the PVA film was dissolved with water. In the same manner, multiple nanosheets were overlapped over the incision. The hydrostatic pressure of glycerin solution (glycerin : water ratio = 2 : 3 (w/w)), which has a similar viscosity to mammalian blood, was measured by water head difference every 10 mmHg. The bursting pressure for each multi-overlapped nanosheet against hydrostatic pressure through the incision was evaluated. Each measurement was performed six times.

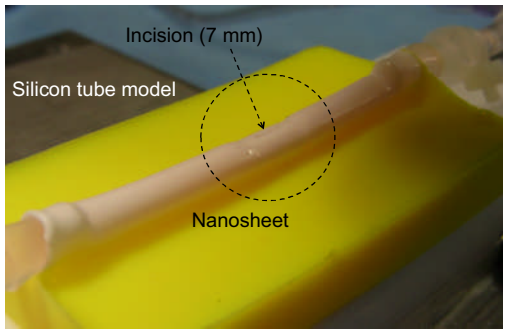

Fig. 4.3 Macroscopic image of silicon tube model covered with nanosheet.

A single layer of polysaccharide nanosheet secured an incision in a silicon tube maximally at 22 ± 4 mmHg (Fig. 4.4), although it did not resist leakage at 30 mmHg. However, overlapping two layers of nanosheets resisted leakage at 30 mmHg, suggesting an augmentation of durability by simply overlapping the nanosheets. In line with this, the

hydrostatic durability of the nanosheets was gradually augmented concomitant with an increase in the number of thenanosheets, and it measured at 80 ± 6 mmHg with four layers of nanosheets. Because hydrostatic pressure of the central veins is usually less than 20 mmHg [12], the data of the silicon tube model suggest that treatment with a single nanosheet is not enough to completely stop the bleeding from the IVC. However, the multi-overlapping process improved the hydrostatic durability of the polysaccharide nanosheet. This result suggests that multi-overlapping therapy, especially when two or three polysaccharide nanosheets are overlapped, stops the IVC hemorrhage. In one case where the distal clamp was accidentally removed from the IVC before the release of the proximal clamp, the increased local venous pressure blew out the polysaccharide nanosheet. In this case, re-overlapping of the attached nanosheets immediately stopped the bleeding again. Thus, overlapping therapy is an on-demand and versatile approach to stop venous bleeding.

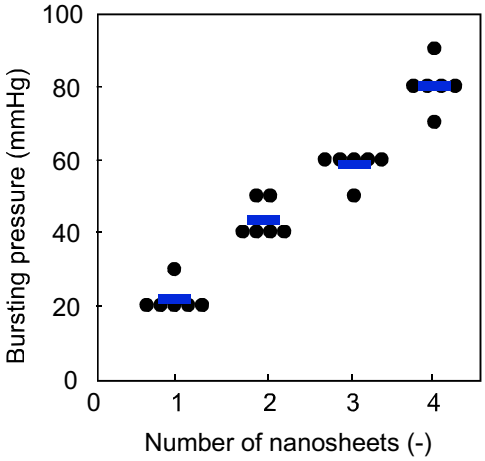

Fig. 4.4 The relationship between the number of multilayered nanosheets and bursting hydrostatic pressure. *Closed circles* are the measured value. *The line* represents the average value.

3.2. Physiological stability test

The physiological stability from the point of the film thickness was evaluated by ellipsometry in PBS (pH 7.4, 37 ^{o}C). Data were expressed as the mean values ± standard deviation. Regarding the degradability of the polysaccharide nanosheet in physiological conditions (at 37 ^{o}C in PBS),

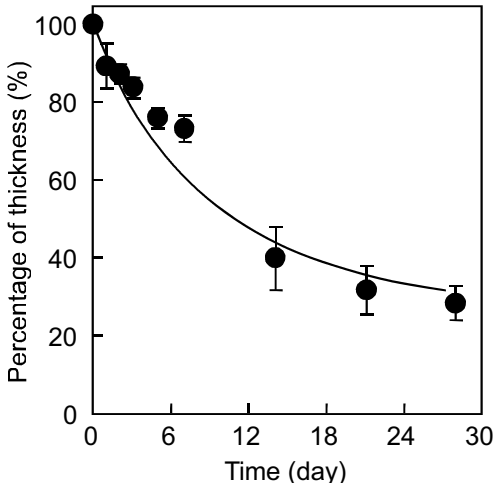

Fig. 4.5 Degradable profile of the nanosheet in phosphate-buffered saline (pH 7.4; 37^{o}C) as a function of the remaining film thickness (%).

the thickness of the 75 nm nanosheet was gradually decreased (Fig. 4.5). However, a thickness of more than 70% was maintained for 7 days.

4. Overwrapping therapy using polysaccharide nanosheet for IVC injury

4.1. Preparation of rabbit IVC injury model

Twelve New Zealand White rabbits were anesthetized using 50 mg of ketamine and 20 mg of xylazine as an intramuscular injection, and maintained on pent barbiturate (15 mg/kg) via the marginal ear vein. A midline incision was made in the lower part of the abdomen. Thereafter, the IVC was isolated from the peripheral connective tissue and at least 3 cm was laid on a colored vinyl sheet in order to clarify the injury site (Fig. 4.6 (a)). The blood flow of the IVC was temporally occluded by two bulldog force ps. Subsequently, a 7 mm longitudinal incision was made in the wall of the IVC (Fig. 4.6 (b)).

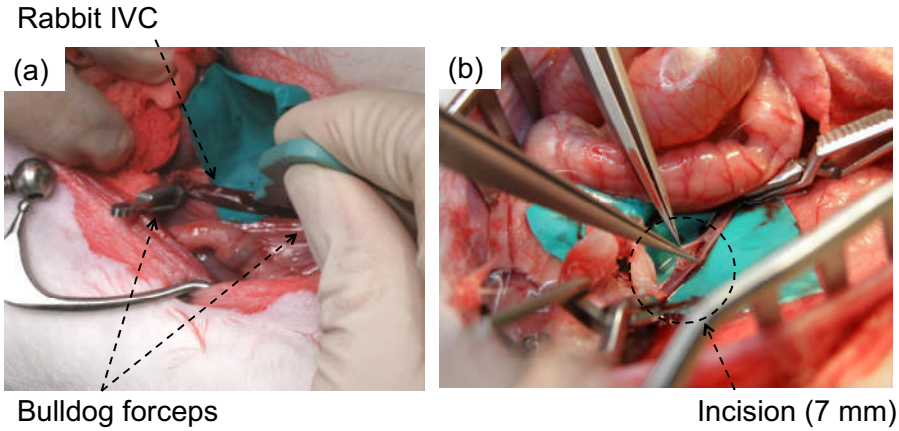

Fig. 4.6 (a) Cutting the inferior vena cava (IVC) to make a 7-mm longitudinal perforation injury. (b), Cutting site of the IVC vessel wall.

To test whether injured vessels could re-seal without any additional treatment, the injured vessel was manually compressed with gauze for 5 minutes (n=3). When the compression was released, severe venous bleeding was observed. Venography also showed a large amount of hemorrhage from the incised IVC. Thus, hemorrhage did not spontaneously stop after five minutes of manual compression in this rabbit IVC model.

4.2. Overlapping therapy using single layer of nanosheet

The rabbits were then divided randomly into the following two groups: the nanosheet group and the control group. In the nanosheet group (n=6), after cutting the vessel wall, residual blood was completely removed from the clamped site of the IVC (Fig. 4.6 (b), 4.7 (a)). Thereafter, a piece of nanosheet, with an area of 1 cm^2 (1 cm x 1 cm), was settled and placed over the incision (Fig. 4.7 (b)). Subsequently, saline was dropped onto the nanosheet in order to dissolve the supporting PVA film. After removing the PVA film, the proximal bulldog was unclamped, followed by the distal clamp. In control rabbits (n=6), the cut IVC was repaired using a 10-0 monofilament suture that was 15 to 40 μm in diameter (KONO SEISAKUSYO, Ichikawa, Japan). After surgery, the abdominal cavity was washed with saline and the wound was closed.

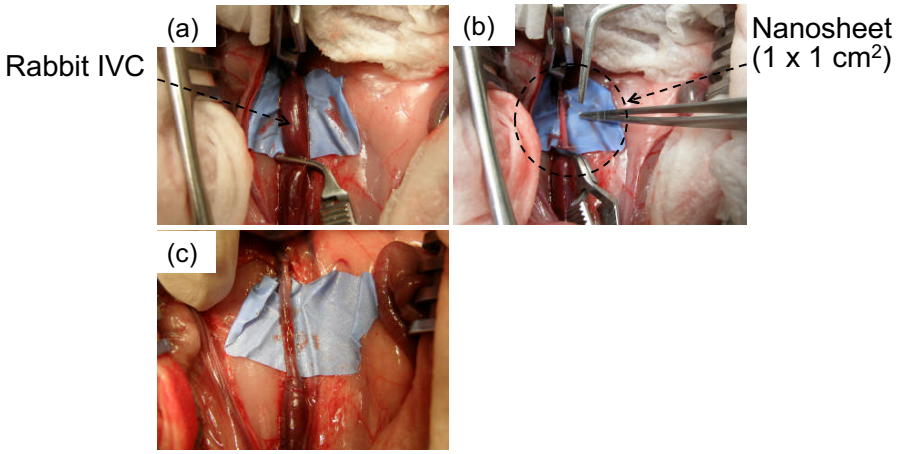

Fig. 4.7 (a) Clamping the IVC. (b) Overlapping a single layer of the nanosheet onto the injured site. (c) Blood flow refilling immediately after declamping. Representative data are shown from two rabbits receiving overlapping treatment of a single-layered nanosheet with similar results.

Overlapping therapy using the single layer of nanosheet on the IVC incision site effectively stopped bleeding from the injured site in two of six rabbits (33.3%) (Fig. 4.7 (c)). Nevertheless, a small amount of hemorrhage (oozing) was still observed at the injured site after application of a single nanosheet in the other four rabbits.

4.3. Multi-overlapping therapy using the nanosheets

If the bleeding did not stop completely (Fig. 4.8 (a)), “multi-overlapping therapy” was performed (Fig. 4.8 (b)). We repeatedly overlapped the nanosheet on the bleeding/oozing site until the bleeding stopped completely.

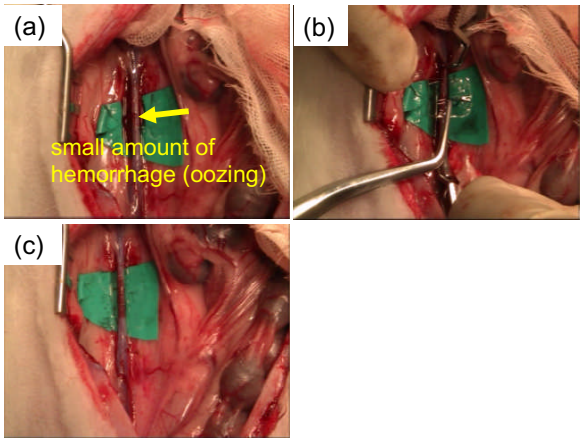

Fig. 4.8 (a) Oozing from the IVC overlapped with a single-layer nanosheet. An arrow indicates the oozing site. (b) Multilayered overlapping of two polysaccharide nanosheets on the injured site. (c) Blood flow refilling immediately after declamping. Representative data are shown from two rabbits receiving over- lapping treatment of a double-layered nanosheet with similar results.

The bleeding was completely stopped by the additional overlapping of one, two, or three layers of nanosheets, respectively (Fig. 4.8 (c)). Ultimately, two rabbits received double-layered nanosheet therapy, another one received triple-layered therapy, and the other one received quadruple-layered therapy. At most, four pieces of overlapping nanosheets were required to completely stop the bleeding from the IVC incision site.

4.4. Venografic and histlogical examination

Venograms were examined to evaluate vessel patency, stenosis and thrombosis in rabbits one month after overlapping nanosheet treatment or suture repair. Venograms were performed by injecting iodide contrast agents (5 mL of Iopamiron 370, Bayer Healthcare, Tokyo, Japan) via the right femoral vein. Thereafter, the rabbits were euthanized with an intravenous injection of pentbarbiturate. The IVC, including the surgical site, was excised and

fixed in 10% neutral buffered formalin for 2 days. Slides were prepared from the fixed specimens and stained with hematoxylin and eosin.

Acute phase venograms showed no blood leakage from the nanosheet attached site in any rabbit. The manipulated IVC, however, tended to be narrow because the blood flow escaped to collateral veins due to the temporary mechanical obstruction of the IVC (Fig. 4.9 (a), (b)). One month after surgical intervention, venograms were repeated and normal blood flow in the IVC as well as normal vessel morphology was demonstrated in both the nanosheet-treated and suturing repair rabbit groups. There was no stenosis, thrombosis, or aneurysm in the treated IVC site in either group (Fig. 4.9 (c), (d)).

(a) (b)

(c)

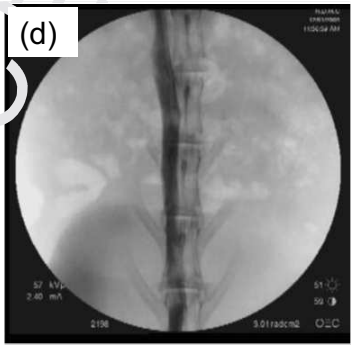

Fig. 4.9 (a) Venographycal images of 10 minutes after (a) nanosheet-overlapping therapy or (b) suture repair. (Collateral blood flow along the IVC is also observed (arrows).) Venographycal image of 1 month after (c) nanosheet-overlapping therapy or (d) suture repair.

The pathological findings also indicated complete wound healing with re-endothelialization of the injured vena cava in both groups (Fig. 4.10). No adhesive lesions were observed around the manipulated IVC site in nanosheet-treated rabbits, and the IVC was as easily isolated from the peripheral soft tissues as at the first dissection (Fig. 4.10 (a)). In contrast, the IVC treated with conventional suturing repair showed severe adhesions. In this

case, it was very difficult to isolate the manipulated IVC from the aorta and surrounding connective tissues (Fig. 4.10 (b)). Neither thrombosis, pseudo-aneurysm or an inflammatory tissue response was found around the nanosheet attachment site in the nanosheet group (Fig. 4.10 (c)). Conversely, a severe inflammatory tissue response was found around the vessel, especially adjacent to the stitch area, in the suturing repair group (Fig. 4.10 (d)).

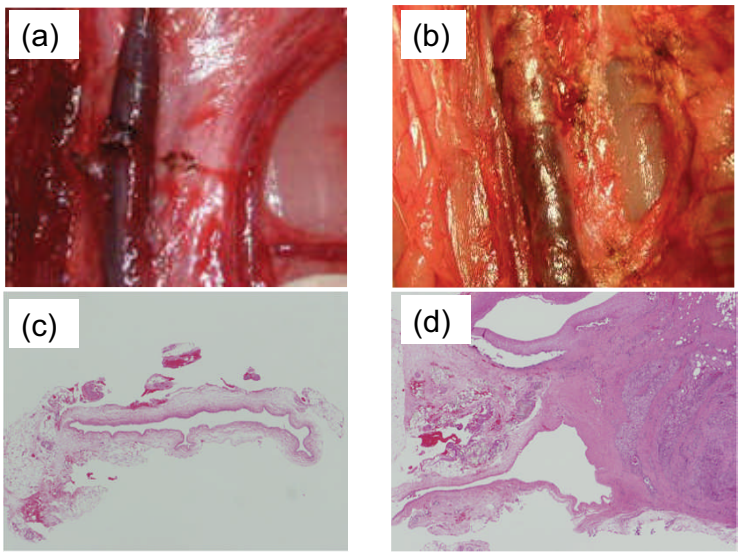

Fig. 4.10 Injured inferior vena cava (IVC) site 1 month after (a) nanosheet-overlapping therapy (b) suture repair. Histological findings of the injured IVC site 1 month after (c) nanosheet-overlapping therapy or (d) suture repair (H-E staining).

In general, wound healing takes three steps: 1) hemostasis and inflammation (days 0-6), 2) proliferation (days 4-14), and 3) maturation and remodeling (beyond day 8) [13]. Therefore, in the current rabbit model, a 28 day observation period is appropriate to confirm the wound healing process and to detect complications of venous lacerations. Indeed, the nanosheet-treated rabbits showed complete wound healing without thrombosis or pseudo-aneurysms. Although traumatic venous aneurysms or pseudo-aneurysms seldom occur in clinical settings [14, 15], there are a few case reports of such complications following venous catheterization [16, 17]. These complications were caused acutely by percutaneous puncture, which is different from the present situation because venous injury was immediately repaired with overlapping nanosheets or suturing. As for long-term complications, venous

aneurysms or pseudo-aneurysms are sometimes caused by high pressure originating from aortic dissection [18] or vein graft trouble after by-pass surgery [19, 20]. These situations also appear to be somewhat different from the present model. However, we cannot entirely rule out the possibility of the late complications such as venous aneurysms beyond 28 days. Further long-term studies should be performed to investigate the occurrence of such late complications.

The procedure of the nanosheet overlapping therapy is quite simple and quick for the repair of vessel wall injuries compared to conventional suturing repair. In the present study, the overlapping nanosheet therapy took two or three minutes to finish without any complicated techniques. Trauma injuries are complicated, but this simple and easy repair procedure may be suitable for emergency conditions. Moreover, there is also no concern about the risk of infectious disease transmission, as the materials do not contain biological materials such as proteins. This is unique aspect of the nanosheet, which is different from other artificial hemostatic sheets that contain human-derived coagulating molecules such as fibrin, fibrinogen, and/or recombinant thrombin. These may assist hemostasis but do not directly stop bleeding.

However, there is limitation. We simply evaluated whether the nanosheets can assist healing of a vessel laceration while enduring venous pressure in the acute phase and also whether they induce an inflammatory tissue reaction around the injured site in the chronic phase. The injury model may not be a typical model of severe venous injury, because traumatic venous injuries are often complex crush injuries with multiple points of injury in which hypothermia or coagulopathy are induced. Further studies are required to evaluate the effect of nanosheet therapy on venous injuries with multiple traumas.

5. Summary

We demonstrated that multi-overlapping therapy using polysaccharide nanosheets with a thickness of 75 nm stopped major venous bleeding rapidly and conveniently without adverse effects in the immediate and chronic phases following injury. Hydrostatic durability of the polysaccharide nanosheet was increased when a number of nanosheets were overlapped. Multi-overlapping therapy effectively sealed and stopped the bleeding from an injured IVC without significant inflammatory tissue response, while conventional suturing repair induced a severe inflammatory response.

References

55) J. S. Paul, T. P. Webb, C. Aprahamian, J. A. Weigelt, *J. Trauma.*, **69**, 1393 (2010).

56) E. Degiannis, G. C. Velmahos, R. D. Levy, I. Souter, C. A. Benn, R. Saadia, *Ann. R Coll. Surg. Engl.*, **78**, 485 (1996).

57) J. A. Asensio, S. Chahwan, D. Hanpeter, D. Demetriades, W. Forno, E. Gambaro, et al., *Am. J. Surg.*, **180**, 528 (2000).

58) N. Hudorovic, *Surgery*, **7**, 158 (2008).

59) S. R. Klein, F. J. Baumgartner, F. S. Bongard, *J. Trauma*., **37**, 35 (1994).

60) J. M. Porter, R. R. Ivatury, S. Z. Islam, A. Vinzons, W. M. Stahl, *J. Trauma,* **42**, 913 (1997).

61) J. A. Carr, K. A. Kralovich, J. H. Patton, H. M. Horst, *Am. Surg.*, **67**, 207 (2001).

62) P. S. Sullivan, C. J. Dente, S. Patel, M. Carmichael, J. K. Srinivasan, A. D. Wyrzykowski, *et al.*, *Am. J. Surg.,* **199**, 500 (2010).

63) J. A. Asensio, P. Petrone, L. Garcia-Nuñez, M. Healy, M. Martin, E. Kuncir, *J. Trauma.* **62**, 668 (2007).

64) T. Fujie, N. Matustani, M. Kinoshita, Y. Okamura, A. Saito, S. Takeoka, *Adv. Funct. Mater.* **19**, 2560 (2009).

65) Y. K. Park, Y. Mita, E. Oki, N. Kanemitsu, Y. Shiraishi, Y. Ishii, T. Azuma, M. Ochi, M. Umezu, *Conf. Proc. IEEE Eng. Med. Biol. Soc.,* **2007**, 2705 (2007).

66) S. Magder, *Crit. Care. Med.,* **34**, 2224 (2006).

67) A. Barbul, Wound Healing. In: Brunicardi FC editor. Schwartz's Principles of Surgery, 8th ed. New York: McGraw-Hill; p. 223-30, (2005)

68) J. J. Hewett, K. S. Freed, D. H. Sheafor, S. N. Vaslef. *AJR Am. J. Roentgenol.,* **172**, 1144 (1999).

69) A. Delgado-Beltran, D. Cubillos, *J. Trauma,* **67**, E75 (2009).

70) A. Kunizawa, M. Fujioka, S. Mink, E. Keller,. *Minerva. Anestesiol.*, **10**, 868 (2010).

71) A. E. Sirvent, R. Enríquez, D. Martínez, A. Reyes, *Nefrologia*, **28**, 654 (2008).

72) R. J. Salem, *Tex. Heart Inst. J.,* **39**, 866 (2012).

73) P. Kallis, B. E. Keogh, M. J. Davies, *Br. Heart J.*, **70**, 189 (1993).

74) S. A. Rahim, S. R. Pitta, C. S. Rihal, *J. Am. Coll. Cardiol.,* **53**, 1918 (2009).

Chapter 4.

Wound protective efficiency of fragmented nanosheet in murine partial-thickness burn model

1. Introduction

The epidermis not only prevents the loss of endogenous fluids but also protects against exogenous microbial invasion. Burn injury results in the loss of a physical barrier to infection, thereby rendering the host susceptible to bacterial infection, in particular burn-wound infections. *Pseudomonas aeruginosa* (*P. aeruginosa*) and methicillin-resistant *Staphylococcus aureus* (MRSA) are the most common bacteria found in these post-burn wound infections [1]. Many researchers have investigated appropriate treatments to reduce the risk of wound infections and to promote wound healing [2–7]. Although the management of full-thickness burn injuries requires skin grafting, partial-thickness burn injury does not always require grafts because this type of injury disrupts the epidermis and part of the dermis, but the regions still retains the potential for reepithelialization.

The management of partial-thickness burn injuries requires acute wound care, pain control, and infection control [2, 8]. Bacterial colonization of burn-injured tissue compromised by inflammation may lead to local invasion and systemic sepsis. Burn wound infection severely impairs reepithelialization and exacerbates pain in the patients with partial-thickness burn injury. If a partial-thickness burn wound does not develop any bacterial infections, the wound can be epithelialized and will heal automatically. Therefore, the prevention of wound infection is important for the care of such patients.

In our previous research, we investigated that the protective properties of the PLLA nanosheet as a wound dressing material against burn wound infection in a mouse model of partial-thickness burn injury (Fig. 5.1) [9]. The PLLA nanosheet appears to provide a barrier to invasion from external microbes. The PLLA nanosheet is an effective dressing material for the management of partial-thickness burn wounds.

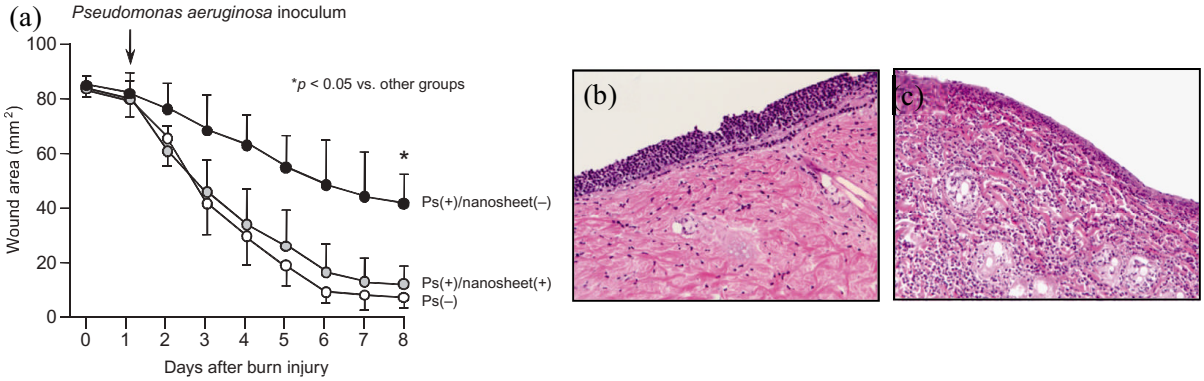

Fig. 5.1 (a) The assessment of burn wound healing. The wound was traced, and the traced area was calculated using the Image J software program. The data are the means ± standard deviations from 10 mice in each group. Histological images of dosal skin of *P. aeruginosa* infected mice (b) with or (c) without nanosheet therapy 4 days after injury.

Although the nanosheet can be tightly covered on various surfaces, it is difficult to cover the large area easily (~m^2 scale). Therefore, in this chapter, we propose i) a one-pot fabrication of freestanding biodegradable nanosheets composed of PLLA, ii) their fragmentation, and iii) a simple patchwork technique using the fragmented nanosheets to effectively wrap different shaped materials. Furthermore, we demonstrate that the fragmented PLLA nanosheets act as a physical barrier against burn wound infection with *P. aeruginosa*.

2. ***Development of fragmented nanosheet***

2.1. Fabrication and characterization of fragmented PLLA nanosheets

A PVA solution (10 wt% in distilled water, 1 mL) was dropped onto the SiO_2 substrates, and then the substrates were spin-coated at 4000 rpm for 20 s followed by drying at 70 ^oC for 90 s. Next, a PLLA solution (1 wt% in CH_2Cl_2, 1 mL) was dropped onto the PVA layer. The substrates were then spin-coated and dried as described earlier. For one-pot preparation of many PLLA nanosheets, the multi-layering process of PVA and PLLA was repeated 25 times with multiple rounds of spin-coating (4000 rpm, 20 s) and drying (70 ^oC, 90 s) (Fig. 5.3 (a)). The resulting substrates were immersed in distilled water at room temperature (RT) overnight to obtain a suspension of freestanding PLLA nanosheets. The dissolved PVA was completely

removed by repeated cycles of centrifugation (1,600 *g*, 10 min, RT, 5 times) and washing with distilled water. Next, the resulting PLLA nanosheets were homogenized at 33,000 rpm for 1–10 min. After centrifugation (1,600 *g*, 10 min, RT, 5 times), we obtained the fragmented PLLA nanosheets (Fig. 5.2 5.3 (b)).

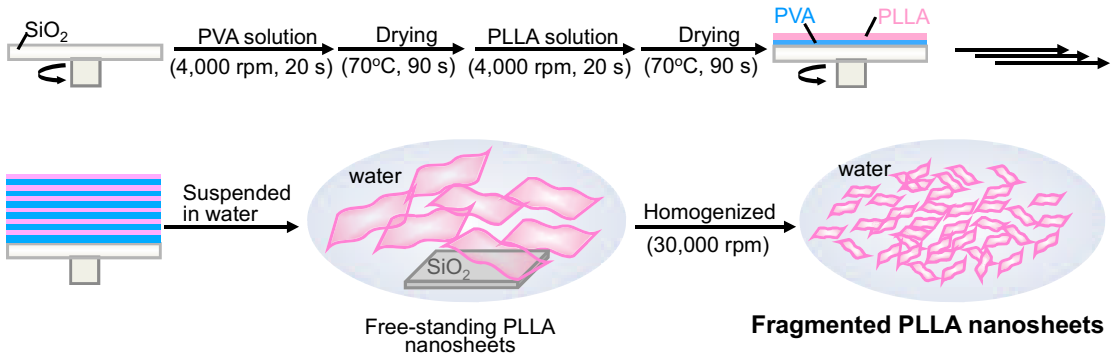

Fig. 5.2 Schematic representation of fragmented nanosheet.

By dissolution of the sacrificial PVA layers between PLLA layers or on the substrate in distilled water, we successfully obtained 25 freestanding PLLA nanosheets (Thickness: 60 ± 6 nm), corresponding to the number of multi-layering processes of PVA and PLLA (Figure 5.3 (a)). The resulting nanosheets maintained the shape and size of the SiO_2 substrate (40 mm x 40 mm) and were transparent and extremely flexible. Consequently, we succeeded in radically improving the productivity of freestanding PLLA nanosheets by a simple combination of a spin-coating-assisted multi-layering process of PVA and PLLA with a peeling technique. When the suspension of the PLLA nanosheets (single-side surface area of PLLA nanosheet: 1.6×10^3 mm^2) was homogenized at 33,000 rpm, they were instantly fragmented. The turbidity and viscosity of the resulting suspension increased with continuing homogenization (Fig 5.3 (b)).

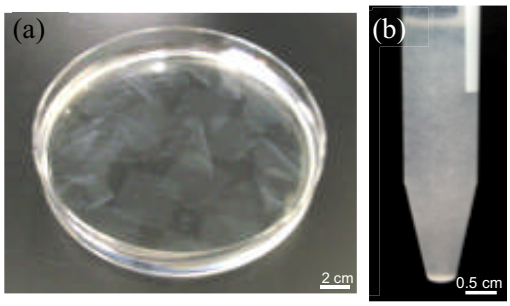

Fig. 5.3 (a) Macroscopic image of 25 pieces of PLLA nanosheet with a thickness of 60 ± 6 nm suspended in water, corresponding to the number of multi-layering processes of PVA and PLLA. (b) Macroscopic image of fragmented nanosheet.

We have previously reported that PLLA nanosheets float on distilled water without any stabilizers because of their hydrophobic properties [10]. Interestingly, however, the fragmented nanosheets can be suspended in their open conformation and do not aggregate by hydrophobic interactions in distilled water, even in the absence of any stabilizers. Fourier transform infrared (FTIR) analysis of the fragmented PLLA nanosheets revealed a band at 3,350 cm^{-1}, corresponding to the O–H stretching vibration mode (Fig. 5.4). This observation suggested that PVA, which is used as a water-soluble sacrificial layer, could be deposited onto the surface of the fragmented PLLA nanosheets during the drying process at 70 ^{o}C to help stabilize the suspension.

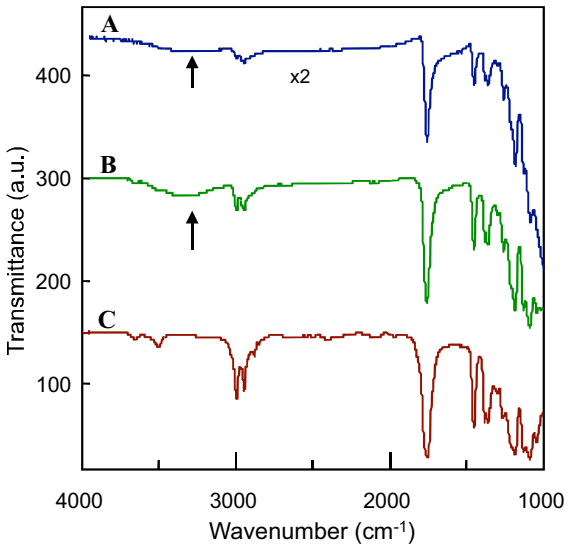

Fig. 5.4 FT-IR analyses of (A) the fragmented PLLA nanosheets, (B) the PLLA nanosheets before fragmentation, which were purified by centrifugation (1,600g, 10 min, RT, 5 times), and (C) PLLA nanosheet prepared directly on a calcium fluoride substrate, which were dried in a desiccator overnight before analyses. Arrows show the band of O-H stretching vibration mode derived from PVA at 3,350 cm^{-1}.

Furthermore, the fragmented PLLA nanosheets can be lyophilized and stably resuspended in distilled water, thereby facilitating their long-term storage as a lyophilized powder (Fig. 5.5).

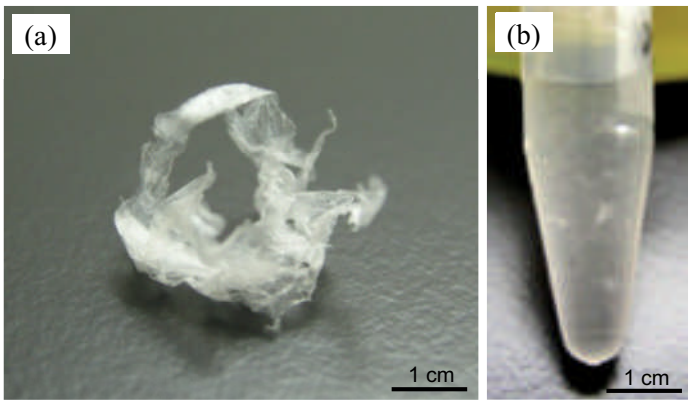

Fig. 5.5 (a) Lyophilized fragmented PLLA nanosheets and (b) resuspension of the lyophilized nanosheets.

2.2. Covering efficiency of fragmented nanosheet

In order to measure the average single-side surface area and concentration of the fragmented nanosheets, 50 μL of a suspension diluted with distilled water at an optimal concentration was dropped onto the bare SiO_2 substrate. The substrates were dried in a desiccator overnight and then analyzed using a stereomicroscope. The average single-side surface area of the fragmented nanosheets and the number of fragmented nanosheets in a 50 μL suspension (i.e., nanosheet concentration) were subsequently calculated using an image analyzer.

The single-side surface area of one fragmented PLLA nanosheet was significantly decreased with increasing homogenization time and reached a minimum at 0.24 ± 0.08 mm^2 at 7 min (Figure 5.6).

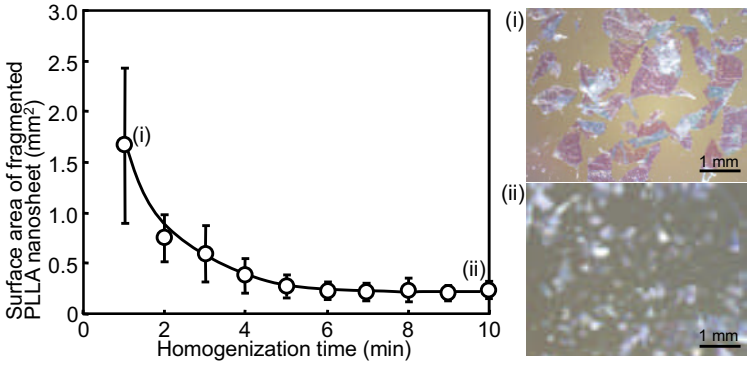

Fig. 5.6 Correlation of the single-side surface area of one fragmented PLLA nanosheet with homogenization time. As a reference, the surface area before homogenization was 1,600 mm^2 (40 mm x 40 mm). The experiment was performed at least three times. Values are given as the mean ± SD (standard deviation). Insets i) and ii): Representative images of fragmented PLLA nanosheets adhered on the SiO_2 substrate after 1 and 10 min homogenization, respectively.

Taking into account the volume (1.44×10^{-14} m^3) and total surface area (4.80×10^{-7} m^2) of the fragmented PLLA nanosheets and the density of PLLA (1.27×10^6 g/m^3) [11-13], a simple calculation gives the specific surface area of fragmented PLLA nanosheets to be 26 m^2/g, corresponding to that of nanoparticles with a diameter of 200 nm (24 m^2/g). However, the PLLA nanoparticles with comparable diameters adhered on the SiO_2 substrate were easily removed from the substrate by simply washing with distilled water (Fig. 5.7 (a)), whereas the

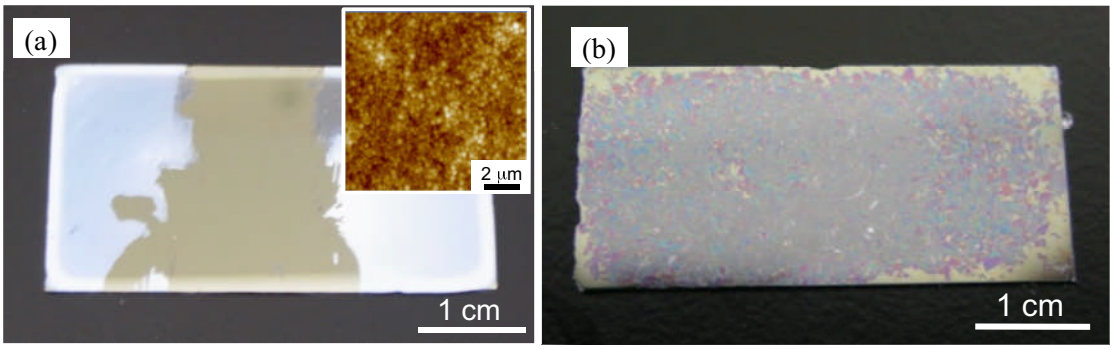

Fig. 5.7 Adhesiveness of (a) PLLA nanoparticles and (b) fragmented PLLA nanosheets with similarly surface area after washing by distilled water. Inset in (a) shows an AFM image of PLLA nanoparticles adhered on the SiO_2 substrate.

fragmented nanosheets were difficult to detach even after fragmentation (Fig. 5.7 (b)). This observation indicates that the nanoparticles, which are being considered as drug delivery carriers for wounds, may not adhere appropriately to the interfaces owing to their small contact area, and the nanosheets, with similarly surface area but enhanced adhesion properties, may be more appropriate for these applications (Fig. 5.8). This is a characteristic feature of nanosheets.

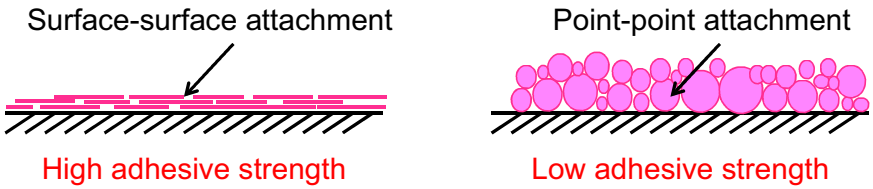

Fig. 5.8 Schematic explanation of the adhesive mechanism difference between fragmented nanosheet and nanoparticles.

2.3. Adhesion and reconstruct behavior of fragmented nanosheet

To explore the adhesion behavior of the fragmented PLLA nanosheets, suspension of the fragmented PLLA nanosheets (50 μL) was dropped onto the SiO_2 substrate and then dried in a desiccator overnight. The macroscopic morphologies of the fragmented PLLA nanosheets adhered on the SiO_2 substrate were photographed using a digital camera. Microscopic morphologies were recorded using a digital microscope and a field emission scanning electron microscope (FE-SEM, Hitachi S-4500 at an accelerating voltage of 5 kV). For SEM images, the substrates were coated with tetroxide (thickness: ca. 10 nm) using an osmium plasma

coater (NL-OPC80, Nippon Laser & Electronics Lab., Nagoya, Japan) prior to observation.

The fragmented PLLA nanosheets firmly adhered onto the substrate in a spread-out conformation (i.e., not aggregated or curled up) even in the absence of adhesive reagents (Fig. 5.9 (a)). Once the nanosheets had dried onto the surface, they were difficult to detach even by scratching with tweezers. The distribution of the nanosheets resembled a "patchwork", which was evident as a sequential series of structural colors on the SiO_2 substrate (Fig. 5.9 (b)). The colors depended on the number of overlaid nanosheets according to thin-film interference theory:[3b] red for a single layer (thickness: ca. 60 nm), blue for double layers (ca. 120 nm), and yellow-green for triple layers (ca. 180 nm). Based on SEM observations, although some wrinkles (not cracks) formed during the adsorption process, the nanosheets were tightly attached (Fig. 5.9 (c)). These results indicate that the fragmented nanosheets consist of a patchwork, where the sheets are strongly adhered to each other in a spread-out arrangement.

Fig. 5.9 Macroscopic (a) and microscopic (b,c) images of fragmented PLLA nanosheets adhered on the SiO_2 substrate obtained using a digital camera, a digital microscope, and a scanning electron micro- scope, respectively.

Next, we examined whether the fragmented PLLA nanosheets could be reconstructed into one continuous nanosheet. The fragmented nanosheets (concentration of 1 x 10^5 sheets/mL) were first cast onto a PTFE plate, which was then dried in a desiccator overnight. The resulting film detached from a PTFE plate was photographed using a digital camera.

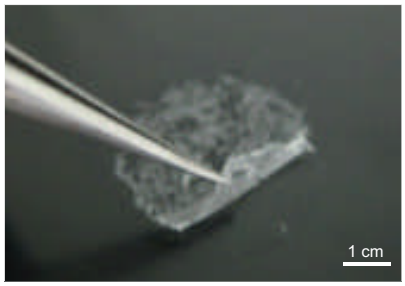

Fig. 5.10 Detachment of fragmented PLLA nanosheets from the PTFE plate.

When fragmented PLLA nanosheets at a concentration above 1 x 10^5 sheets/mL were cast on a PTFE plate, which

has a lower surface energy than the SiO_2 substrate, the sheets could be detached from the plate as a film picked up with tweezers (Fig. 5.10). Hence, the fragmented PLLA nanosheets after casting can be reconstructed as one nanosheet on the substrate.

2.4. Formation of a patchwork of fragmented PLLA nanosheets on several surfaces

To visualize the ubiquitous patchwork of the nanosheets on several irregularly shaped interfaces, the fragmented nanosheets labeled with rhodamine at a concentration of 1 x 10^4 sheets/mL (30 mL) were suspended in a glass beaker. A 18G needle (Termo Co., Tokyo), artificial skin derived from polyurethane resin, and the lower half of a mouse body including the perineum (C57BL/6, 7 weeks old, weight 20 g, Japan SLC, Tokyo) were vertically dipped and lifted into/from the beaker once each cycle and dried at RT for ca. 30 min. Before this procedure, the mice were deeply anesthetized with sodium pentobarbital at a dose of 2.5 mg per body and the hair of the lower half of the mouse body was dehaired with hair removal cream (Shiseido Co. Ltd.).

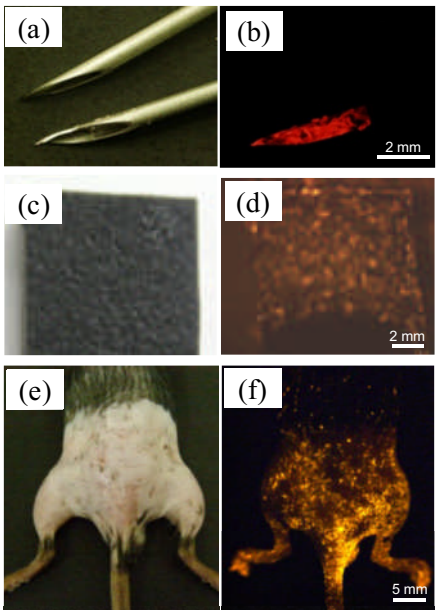

Fig. 5.11 Ubiquitous patchwork of the fragmented PLLA nanosheets labeled with octadecyl- rhodamine on the irregularly shaped interfaces (18G needles (a, b), the lower needle in each case is coated with the nanosheets and the upper one not; artificial skin derived from polyurethane resin (c, d); and mouse skin (e, f)) by a vertical dipping and lifting method. Odd- and even-numbered images were taken under visible light and in the fluorescence mode, respectively.

We investigated the coating properties of the nanoshee t by first labeling it with octadecylrhodamine. Using a vertical dipping and lifting method we were able to demonstrate by fluorescence stereomicroscopy that the labeled fragmented nanosheets efficiently coat several different interfaces, such as an 18 gauge (18G) needle (steel), a human skin model derived from

polyurethane resin (plastics), and the lower half of the mouse body, including the perineum, which constitutes an irregular shape (Fig. 5.11). The nanosheets were barely detectable under visible light, indicating that the ultrathin and flexible fragmented nanosheets adhered along the roughness of the interfaces at the nanometer scale. This is a noteworthy characteristic of nanosheets generated using the patchwork technique when adhered to an irregular surface.

2.5. Covering effect of fragmented nanosheet

In the same manner at 2.3., suspensions of the fragmented PLLA nanosheets (50 μL, average single-side surface area of one fragmented nanosheet: 0.24 ± 0.08 mm^2) at a concentration range from 1 x 10^3 to 3 x 10^4 sheets/mL were dropped onto a part (6 mm x 6 mm) of the SiO_2 substrate and then dried in a desiccator overnight. The covering effect of fragmented PLLA nanosheets (surface coverage) was calculated from data obtained using an image analyzer. The average thickness of fragmented PLLA nanosheets adhering to the SiO_2 substrates was also analyzed in parallel using a surface profiler α-step (KLA-Tencor Co., San Jose, CA). Each experiment was performed at least three times.

We determined the optimal amount of fragmented PLLA nanosheets for generating a patchwork. The nanosheets were randomly adsorbed on the substrate in a spread-out manner as described above. With increasing concentration of the nanosheet suspension (1.0, 3.3, 5.0, and 6.7 x 10^3 sheets/mL), the surface coverages (83 ± 7, 89 ± 1, 97 ± 1, and 99 ± 1%, respectively) and average thicknesses (74 ± 29, 79 ± 31, 99 ± 44 and 124 ± 52 nm, respectively) of the patchwork gradually increased (Fig. 5.12). However, the coverage did not reach 100%, although portions of the nanosheets started to be overlaid with each other. At 8.3 x 10^3 sheets/mL, the coverage did reach 100% and the average thickness of adhered nanosheets was calculated to be 244 ± 56 nm, corresponding to 3–5 layers of fragmented

nanosheets (Fig. 5.12). Above this concentration, the surface coverage was maintained at 100% and the thicknesses of the resulting nanosheets increased proportionally. Based on these measurements we calculated that 415 fragmented nanosheets, which had a total single-side surface area of approximately 100 mm^2, were applied to a SiO_2 substrate to cover an area of 36 mm^2. Consequently, we judged that a perfect patchwork could be achieved by applying a three-fold excess of single-side surface area of nanosheets over that of the desired patchwork surface area.

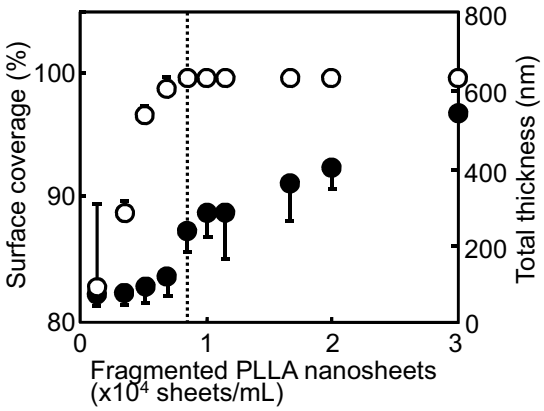

Fig. 5.12 Correlation of surface coverage (empty circles) and thickness (filled circles) of fragmented PLLA nanosheets on SiO_2 substrate with their concentration.

3. Wound protective treatment using fragmented nanosheet

3.1. *In vitro* bacterial permeability assay

A suspension of fragmented PLLA nanosheets (50 μL) at a concentration of 8.3 x 10^3 sheets/mL was dropped onto the outside of a Transwell® Membrane (TM, diameter: 6.5 mm, ϕ = 8 μm) (Fig. 5.13). Accelerated permeability measurements of *P. aeruginosa* were made using three additional large pores (diameter: 1.2 mm each), corresponding to a total area of 3.4 mm^2. The TM coated with fragmented nanosheets was positioned across a 24-well plate, which was filled with 100 and 600 μL of RPMI-1640 medium containing a 10% (v/v) fetal bovine serum (FBS; without antibiotic) in the inner and outer compartments, respectively. A

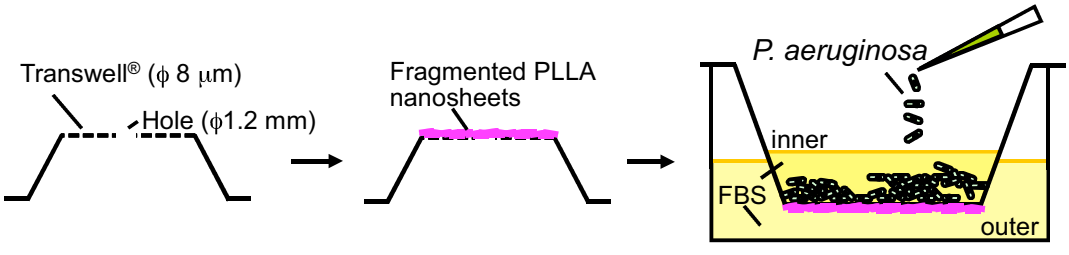

Fig. 5.13 Schematic representation of the bacterial permeability assay.

10 μL suspension of *P. aeruginosa* (1×10^8 CFU/mL) was carefully added to the inner compartment and then cultured for 6 h. The number of bacteria in the outer well that had passed through the nanosheet-coated TM was subsequently determined. A control TM was also made using three additional pores without any coating. Each experiment was performed at least three times. Values are given as the mean ± standard error of mean (SE). Microscopic morphology of the TM surface after coating with the fragmented nanosheets was recorded using a scanning electron microscope (VE-9800, Keyence Co., Osaka, Japan) at an accelerating voltage of 1 kV.

We evaluated whether the patchwork of fragmented PLLA nanosheets could act as a practical physical barrier against burn wound infection. *P. aeruginosa* is a common cause of such infections. The fragmented PLLA nanosheets (8.3×10^3 sheets/mL, 50 μL) were allowed to adhere on the surface of the TM under the conditions required for the perfect patchwork as described above.

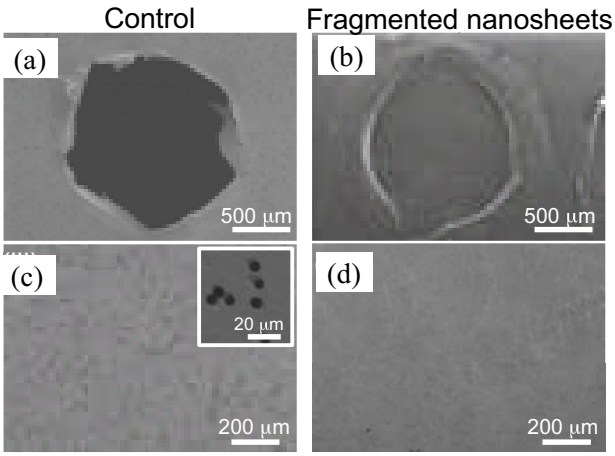

Fig. 5.14 SEM images of TM coated with fragmented PLLA nanosheets (b, d) and TM only (a,c). Images (a) and (b) show the region around the additional pore, whereas images (c) and (d) show the region of the intrinsic pores. Inset in (c): High-magnification image of (d).

Interestingly, microscopic observations of the surface of the TM revealed that the fragmented nanosheets could be used to generate a perfect seal to cover not only the intrinsic pores of TM (8 μm diameter) but also additional pores of 1.2 mm diameter, which are much larger than the dimensions of the fragmented nanosheets (Fig. 5.14).

As a result of *in vitro* test, the number of *P. aeruginosa* passing through the control TM to the outer well was calculated to be $7.7 \pm 1.7 \times 10^6$ CFU/mL 6 h after culturing (Fig. 5.15).

However, the number of bacteria passing through the TM coated with fragmented nanosheets (0.33 ± 0.14 x 10^6 CFU/mL) was significantly lower than that of the control TM. The bacterial counts in the inner wells of the nanosheet-coated TM and control TM were similar (i.e., 14.3 ± 1.5 x 10^6 CFU/mL vs.11.8 ± 2.3 x 10^6 CFU/mL, respectively). These results demonstrate that the fragmented nanosheets can form an effective barrier against penetration by *P. aeruginosa*. Taken together, our results indicate that the fragmented nanosheets can be formed into a single nanosheet that acts as a physical barrier to bacterial permeation.

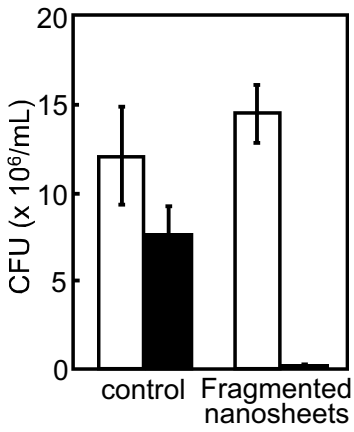

Fig. 5.15 *In vitro* barrier effect of fragmented PLLA nanosheets adhered on the TM. The bacterial cell count in the outer and inner wells was determined after 6 h and is represented by the black and white columns, respectively.

3.2. *In vivo* therapeutic barrier effect of the fragmented PLLA nanosheets

All animal studies were approved by the Animal Research Committee of the National Defense Medical College. Male C57BL/6 mice (7 weeks old, weight 20 g, Japan SLC) were studied. The mice were deeply anesthetized with sodium pentobarbital at a dose of 2.5 mg per body and their dorsal hair was clipped and depilated with a hair removal cream (Shiseido Co. Ltd.). After this procedure, dorsal skins of mice were exposed for 4 s to water heated to 70^{o}C (Fig. 5.16).[6b] The burn area was controlled to be approximately 20% of the total body surface area. The suspension of fragmented nanosheets (1.4 x 10^4 sheets/mL, 30 μL) was dropped on the site of the dermal burn wounds (1 cm circle) and then dried for approximately 5 min. Next, a suspension of *P. aeruginosa* (1 x 10^7 CFU/μL, 10 μL) was carefully dropped on the nanosheets and the mice were wrapped with an OpSite Flexifix transparent film roll (Smith & Nephew Wound Management KK, Tokyo). As a negative control, we induced SDB

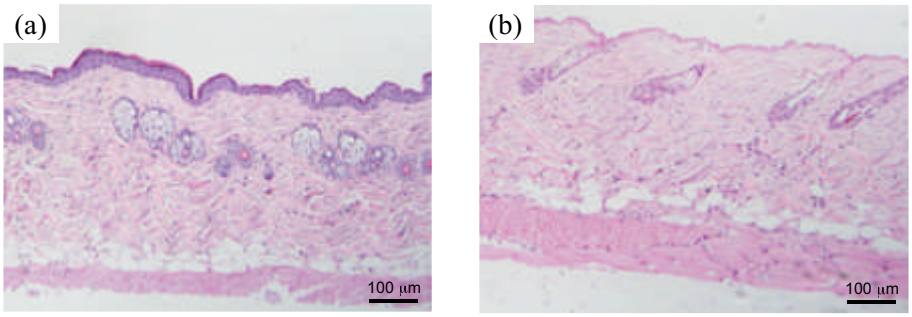

Fig. 5.16 Histological observation of dermal skin before (A) and after (B) treatment with hot water (70°C) for 4 s.

injury in mice but did not treat them with a fragmented-nanosheet coating. Skin was sampled from the mice 3 or 6 days after treatment with fragmented nanosheets, fixed with 10% formaldehyde, and then stained with H&E. To examine the barrier effects of the repeated nanosheet-pachwork, skin with SDB-induced injury was coated on day 1 with the fragmented nanosheets (1st patchwork: 1.4 x 10^4 sheets/mL, 30 μL) and were wrapped with an OpSite film roll. On day 3 after medical intervention, the region of the nanosheet-patchwork was coated again with the nanosheets (2nd patchwork) or not, and then *P. aeruginosa* (1 x 10^7 CFU/μL, 10 μL) was dropped onto the area and the skin was wrapped with an OpSite film roll again. Skin samples were then taken from the mice on day 6 after treatment with fragmented nanosheets, fixed with 10% formaldehyde, and then stained with H&E. Each experiment was performed at least three times.

The suspension of the fragmented nanosheets was simply dropped onto the region of the SDB and then dried for 5 min. SEM observations clarified that the fragmented nanosheets perfectly wrapped the site of burn injury (Fig. 5.17 (a), (b)). This finding indicates that the flexible fragmented nanosheets adhere not only onto flat interfaces such as a SiO_2 substrate and membranes but also onto uneven interfaces such as skin, resulting in a perfect patchwork. Next, we tested the effectiveness of the seal by carefully dropping a suspension of *P. aeruginosa* onto the region of nanosheet-patchwork. Skin samples were then taken from the mice 3 days after treatment of fragmented nanosheets for histological observations.

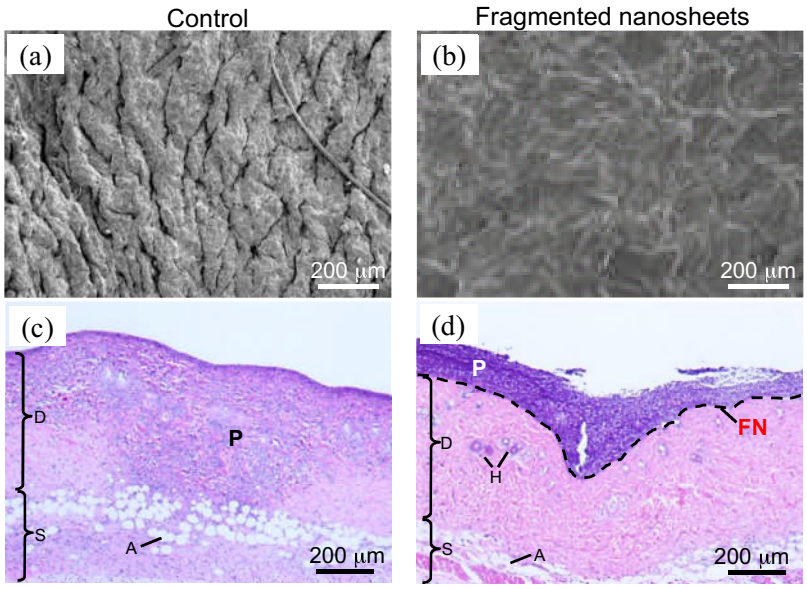

Fig. 5.17 *In vivo* therapeutic barrier assay. a,b) SEM images of SDB-induced skin injury before (a) and after (b) patchwork treatment with the fragmented nanosheets. This observation shows that the fragmented nanosheets could wrap the uneven skin with SDB-induced injury. c,d) Histological images stained with H&E, showing the skin with SDB-induced injury without (c) or with (d) the nanosheet-patchwork. The skin samples were taken from the mice 3 days after the application of *P. aeruginosa*. The letters A, D, FN, H, P, and S in the histological images indicate adipose tissue, dermis, fragmented nanosheets, hair root, *P. aeruginosa*, and subcutaneous layer, respectively.

Interestingly, the *P. aeruginosa* stained in blue-purple with hematoxylin and eosin (H&E) remained on the dermis and did not migrate into the dermis of nanosheet-patchwork-protected dorsal skin with SDB-induced injury (Fig. 5.17 (d)). In the case of the negative control (dorsal skin without a coating of fragmented nanosheets), the *P. aeruginosa* migrated into both the dermis and subcutaneous layer, meaning *P. aeruginosa* infection (Fig. 5.17 (c)). Six days after treatment with fragmented nanosheets, however, the skin was infected with *P. aeruginosa* despite the nanosheet patchwork (Fig. 5.18). In fact, there were some pores and cracks in the nanosheets and their partial detachment in almost all cases even before *P. aeruginosa* was applied suggests that the nanosheets may be degraded by tissue

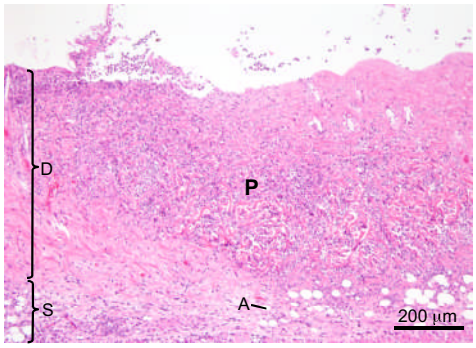

Fig. 5.18 *In vivo* therapeutic barrier assay of the fragmented PLLA nanosheets on day 6 after treatment of fragmented nanosheets.

fluid exuded from the burn wound (Fig.5.19). On the other hand, the surface morphology of the nanosheets was maintained for at least 3 days. Consequently, the single patchwork of the fragmented nanosheets could act as an excellent barrier for burn wound treatment to prevent *P. aeruginosa* infection for at least 3 days.

We tested whether the barrier effect could be maintained for longer periods. To this end, we proposed the repeated patchwork treatment of the fragmented nanosheets as follows: skin with SDB-induced injury was sealed with fragmented nanosheets (1st patchwork). On day 3 after treatment with fragmented nanosheets, the region of nanosheet-patch- work was sealed or not with the nanosheets again (2nd patchwork), and then asuspension of *P. aeruginosa* was applied to the same region. The histological observations on day 6 revealed that the burn skin treated with the 2nd patchwork certainly prevented the infection, patchwork certainly prevented the infection, whereas the skin without the 2nd patchwork treatment was

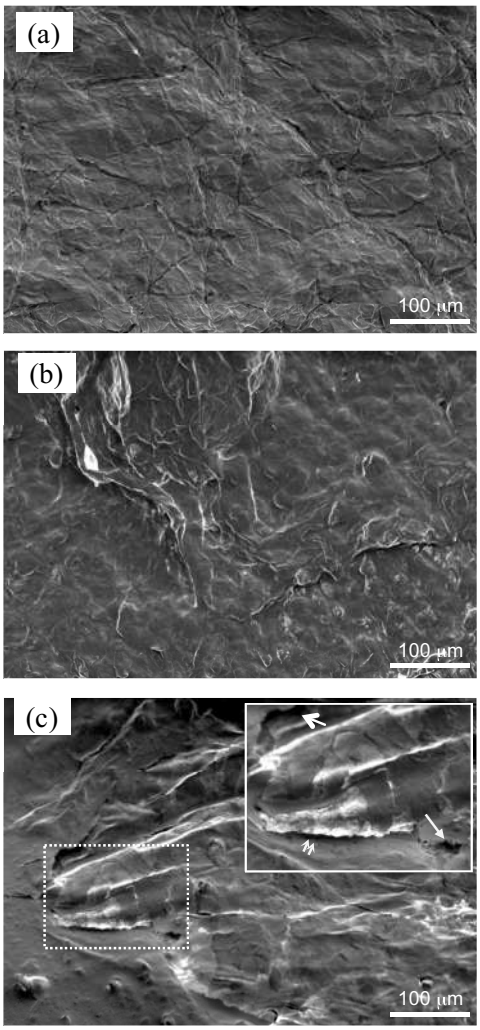

Fig. 5.19 Morphologies of fragmented PLLA nanosheets adhered to superficial dermal burn-induced skins on day 3 (b) and day 6 (c). Image (a) shows the burn-skins before nanosheet-patchwork. Image (b) shows that there were no cracks and pores on the nanosheets adhered on the skins in spread out conformation. In inset of image (c), there were some cracks (opened arrow) and pores (closed arrow) on the nanosheets and their partial detachment (doubled arrow). The inset shows magnified view as shown in dotted square.

significantly infected with *P. aeruginosa* as expected (Fig. 5.20). Consequently, the repeated patchwork treatment with fragmented nanosheets repaired the degraded 1st patchwork. This suggests that an additional patchwork treatment on day 3 could potentially prevent infection

for a longer period. Moreover, we were also able to demonstrate that the fragmented nanosheets were sufficiently coated on the fingertips of a mouse by simple dipping and lifting only. This patchwork technique using fragmented nanosheets shows immense potential as a novel burn wound therapy for both relatively flat dermal skin and skin with an irregular surface shape.

The fragmented nanosheet can cover the huge and complex surfaces. The standard nanosheet can't be covered on their surfaces. Moreover, not only dipping process but also cast process can reconstruct the fragmented nanosheet to bulk one. Reconstructed nanosheet perform similar protection to standard nanosheet. Therefore, the fragmented nanosheet is effectively cover the wound site. However, the reconstruction process takes time because the dispersion solvent is water (ca. 5-10 min). Thereby, the quick-drying dispersion will be developed and this material will be performed more effectively covering onto the various surfaces.

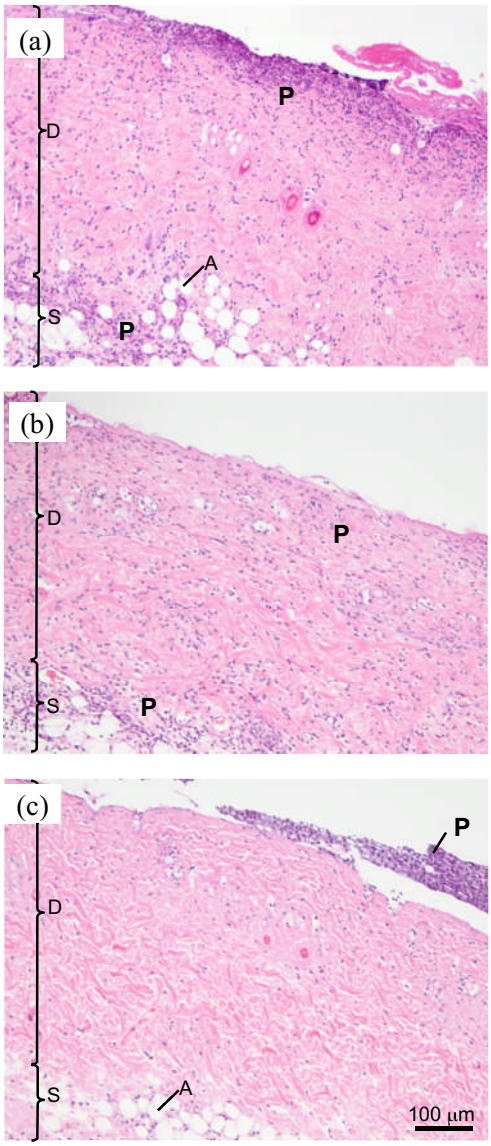

Fig. 5.20 Histological images show the burn-induced skins on Day 6 without (a) or with (b) the single nanosheet-patchwork, respectively. On day 1, burn-induced skins were not or were coated with the fragmented nanosheets. On day 3 after treatment of fragmented nanosheets, *P. aeruginosa* was applied. The skin samples were then taken from the mice on day 6. (c) Histological image of the burn-induced skins on Day 6 with the repeat nanosheet-patchwork. On day 1, burn-induced skin was coated with the fragmented nanosheets (1st patchwork). On day 3 after treatment of fragmented nanosheets, the region of nanosheet-patchwork was coated with the nanosheets again (2nd patchwork), and then *P. aeruginosa* was applied.

4. Summary

In conclusion, 25 freestanding PLLA nanosheets with a thickness of 60 ± 6 nm were successfully obtained in one pot by a simple combination of a spin-coating-assisted multi-layering process of PVA and PLLA and a novel peeling technique. The nanosheets were then fragmented to form a stable suspension that could be reconstructed to provide a single continuous film that firmly attaches to various interfaces without the need for any adhesive reagents (“patchwork”). The patchwork of frag- mented PLLA nanosheets displays excellent barrier ability to prevent infection by *P. aeruginosa* during the treatment of burns for 3 days. Moreover, an additional patchwork treatment on day 3 would effectively prolong the period of wound protection against infection. Hence, this material shows great promise as a novel wound dressing for burn therapy and would certainly improve the quality of life by reducing the need for dressings to be changed daily. We are also planning to fabricate fragment nanosheets carrying antibiotics and growth factors to aid the process of wound healing more effectively.

References

75) G. Revathi, J. Puri, B. K. Jain, *Burns,* **24**, 347 (1998).

76) M. C. Kessides, M. K. Skelsey, *Cutis,* **86**, 249 (2010).

77) P. G. Bowler, S. A. Jones, M. Walker, D. Parsons, *J. Burn. Care. Rehabil.,* **25**, 192 (2004).

78) S. N. Hosseini, S. N. Mousavinasab, M. Fallahnezhat, *Burns,* **33**, 776 (2007).

79) V. Edwards-Jones, R. Buck, S. G. Shawcross, M. M. Dawson, K. Dunn, *Burns,* **30**, 772 (2004).

80) A. Piatkowski, N. Drummer, A. Andriessen, D. Ulrich, N. Pallua, *Burns* **37**, 800 (2011).

81) A. D. Sezer, F. Hatipoglu, E. Cevher, Z. Ogurtan, A. L. Bas, J. Akbuga, *AAPS PharmSciTech,* **8**, E1–E8 (2007)

82) D. J. Smith Jr, P. D. Thomson, W. L. Garner, J. L. Rodriguez. *Am. J. Surg*., **167**, 46S–8S (1994).

83) H. Miyazaki, M. Kinoshita, A. Saito, T. Fujie, K. Kabata, E. Hara, S. Ono, S. Takeoka, D. Saitoh, *Wound, Rep, Reg.*, **20**, 573 (2012)

84) Y. Okamura, K. Kabata, M. Kinoshita, D. Saito, S. Takeoka, *Adv. Mater., **21***, 4388 (2009)

85) L. Lao, H. Tan, Y. Wang, C. Gao, *Colloids Surf., B,* **66**, 218 (2008)

86) P. X. Ma, R. Zhang, *J. Biomed. Mater. Res.,* **56**, 469 (2001)

87) K. Van de Velde, P. Kiekens, *Polym. Test.,* **21**, 433 (2002)

Chapter 5.

Therapeutic efficiency of antimicrobial loaded nanosheet in murine full-thickness burn with infection model

1. Introduction

As described chapter 5, burn injuries render the host susceptible to bacterial infection because of the large skin defects that are created. Burn-wound infection often causes systemic sepsis and severe septicemia, resulting in an increase in mortality of burn-injured patients. Therefore, appropriate burn-wound care is important to prevent wound infection and improve patient outcome. Complication of burn-wound infection is thus considered as a serious problem in the care of severely burn-injured patients. Currently, such patients are treated by debridement to remove as much of the source of infection as possible, combined with wound dressing and, if required, tissue grafting [1]. However, it is difficult to heal ‘‘full-thickness burns’’. In general, the current standard treatment of a full-thickness burn is tissue grafting. Thus, it is important to inhibit bacterial infection until tissue grafting can be performed.

In this study, we investigate the clinical efficacy of nanosheets that were loaded with the antibiotic tetracycline (TC-nanosheets) as a wound-protective material for full-thickness burn-wound infection in a murine model. In the previous study, we demonstrated the fabrication of antibiotic-loaded nanosheets, which were found to be effective for the treatment of tissue defects in the murine gastrointestinal tract (Fig. 6.1) [2]. In the case of intra-abdominal lesions, it is necessary to close the puncture and inhibit bacterial infection. However, in the case of full-thickness burns, it is necessary to protect the wound site and inhibit bacterial infection until tissue grafting. Therefore, covering and inhibiting bacterial infection using a TC-nanosheet is required for the treatment of both intra- abdominal lesions and full thickness burns. Moreover, we reasoned that the high transparency of the TC-nanosheet would be an advantage for wound management. When the TC-nanosheet

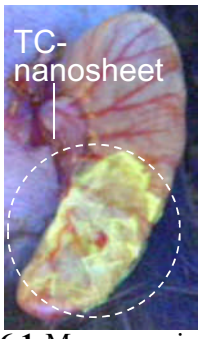

Fig. 6.1 Macroscopic image of murine cecum covered with TC-nanosheet under illuminating black light.

covers the burn-wound infection site, it is possible to inhibit bacterial infection locally, resulting in a significant improvement in mortality. The high flexibility of the TC-nanosheet enables the wound site to be effectively covered with the nanosheet. Moreover, the transparency of the nanosheet allows the wound to be inspected visually during the period of treatment, which is particularly important for the management of full-thickness burns.

2. Development of antimicrobial loaded nanosheet

2.1. Preparation of TC-nanosheets

Spin-coating-assisted LbL (SA-LbL) assembly was performed by following the method described in our previous report (Fig. 6.2 i) [2]. The 10 pairs of LbL nanosheet was prepared. Next, the resulting LbL film was peeled by means of a water-soluble supporting film method (Fig. 6.2 ii). 0.5 ml of PVA (10 wt.%) aqueous solution was cast on the LbL film and dried, and the resulting material was subsequently peeled from the SiO_2 substrate using tweezers. This bilayered film composed of LbL and PVA layers was turned upside down and placed onto another SiO_2 substrate by facing the PVA side to the surface of the SiO_2 substrate (Fig. 6.2 iii). Then, a TC methanol solution was dropped on the LbL side and dried until the methanol had fully evaporated in vacuo (Fig. 6.2 iv). Finally, a PVAc solution (2 wt.%, 0.5 ml) was spin coated at 4000 rpm for 20 s in order to create a hydrophobic barrier (Fig. 6.2 v). The TC-nanosheet covered with a PVAc layer was used for further study with a supporting PVA film. All procedures were conducted in a clean room (class 10,000 conditions) to avoid contamination.

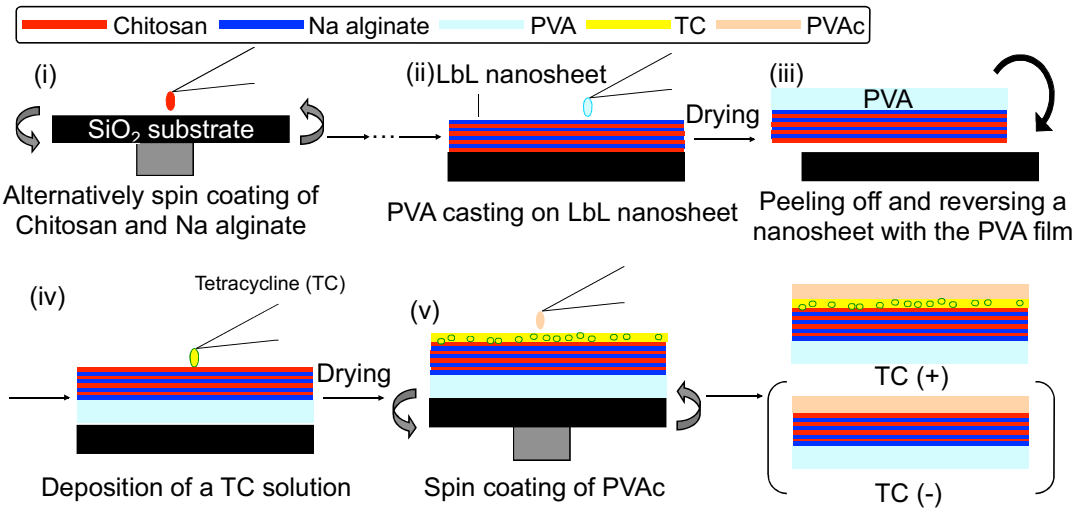

Fig. 6.2 Preparative scheme of TC-loaded nanosheet. (i) Chitosan and Na alginate were alternately spin coated. (ii) PVA was casted onto the LbL nanosheet. (iii) After drying PVA as a supporting layer, the nanosheet was peeled off with PVA and reversed onto the substrate. (iv) TC solution was deposited on nanosheet. (v) After drying to make a TC layer, PVAc was spin coated onto the new layer.

2.2. Characterization of TC-nanosheets

Observation of the TC-nanosheets was undertaken using a Hitachi S-4300 high-resolution scanning electron microscope (Hitachi Co., Tokyo, Japan). Samples were first coated with a platinum layer using an ion-sputtering coater (Hitachi E-1045; 18 mA, 40 s). The TC layer was easily detected by exploiting the autofluorescence of TC (E_x: 380 nm, E_m: 510 nm). The TC layer was also observed by confocal laser scanning microscopy (CLSM). The thickness and surface roughness of TC-nanosheet were measured by surface profiler (α -step, KLA-Tencor Co., San Jose, CA).

Thickness of TC-nanosheet was determined using a surface profiler to be 177 ± 9 nm (Table 6.1). A TC-nanosheet (142 ± 4 nm) without the drug layer (TC (-)) was also prepared as control samples.

Table 6.1 Properties of TC-nanosheets.

Entry	Thickness (nm)	TC[a] (mg/cm^2)	ZOI[b] (mm)
TC (+)[c]	177 ± 9	6.2 ± 0.53	6.6 ± 0.9
TC (-)[d]	142 ± 4	0	0

[a] Tetracycline. [b] Zone of Inhibition.
[c] TC-loaded nanosheet. [d] TC-unloaded nanosheet.

The three-layered structure of the PVAc-TC-nanosheet was confirmed by the cross-sectional SEM and CLSM images. The SEM image showed that the total thickness of

the PVAc-TC-nanosheet was around 150 nm (Fig. 6.3 (a)). A similar thickness (177 ± 9 nm) was measured by the surface profiler. The CLSM images also indicated that TC was incorporated in the layered assembly of the film (Fig. 6.3 (b)).

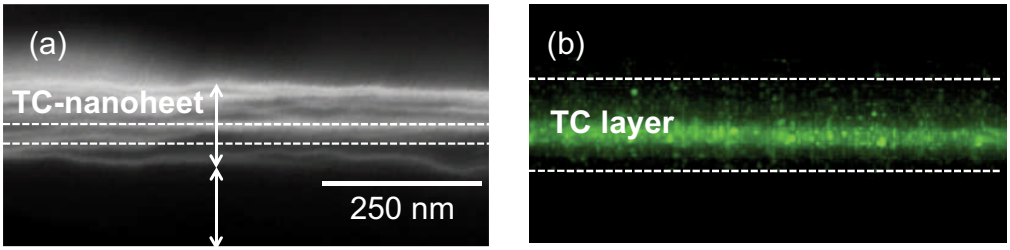

Fig. 6.3 Cross-sectional images of (a) SEM and (b) CLSM observation

The TC-nanosheet was composed of three layers: LbL as a bottom layer, TC as an antibiotic layer and PVAc as a hydrophobic barrier layer. The cross-sectional CLSM image indicated that the TC layer was specifically incorporated between LbL and PVAc. The autofluorescent properties of TC can be exploited to visualize the TC-nanosheet. Other advantages of TC include its broad antibacterial spectrum, affordability and comparatively minor side effects [3]. Therefore, TC is one of the most widely used antibiotics. However, treatment with TC, like other antibiotics, can lead to the emergence of resistant bacteria. Nonetheless, the versatile technique used to construct the antibiotic-loaded nanosheets is applicable to other antibiotics providing their solubility and those of the membrane constituents are appropriate. In this regard, the LbL nanosheet is stable against many solvents including acetone and water. Unless the solvent of the barrier layer (PVAc in this case) dissolves the antibiotics, a three-layered structure, such as LbL/TC/PVAc, can be fabricated. Furthermore, this technique is applicable not just to antibiotics, but to other drugs as well.

3. *In vitro* anti-microbial assay of antimicrobial loaded nanosheet

The antimicrobial effect of the TC-nanosheet was evaluated using the Kirby–Bauer (KB) test. The TC-nanosheets loaded with various amounts of TC were placed on a brain

heart infusion agar on a Petri dish. The KB test was then performed using a culture of *P. aeruginosa* (1 x 10^{10} cfu/mL, cfu = colony-forming units). After incubation for 12 h (37 °C, 5% CO_2) the distance between the edges of the TC-nanosheet and bacterial colony (zone of inhibition (ZOI)) was measured in order to assess the antimicrobial efficacy of the TC-nanosheets.

The antimicrobial effect of the TC-nanosheet was evaluated by the KB test. TC released from the nanosheet inhibited the growth of *P. aeruginosa*, giving a ZOI value of 6.6 mm (Table 6.1). In addition, we optimized the amount of TC on the nanosheet by varying the concentration of antibiotic on a 1 x 1 cm^2 nanosheet. The ZOI plateaued at 10 μg/cm^2 (Fig. 6.4 (a)), suggesting that at higher concentrations of antibiotic a saturated amount of TC had diffused into the medium (Fig. 6.4 (b)).

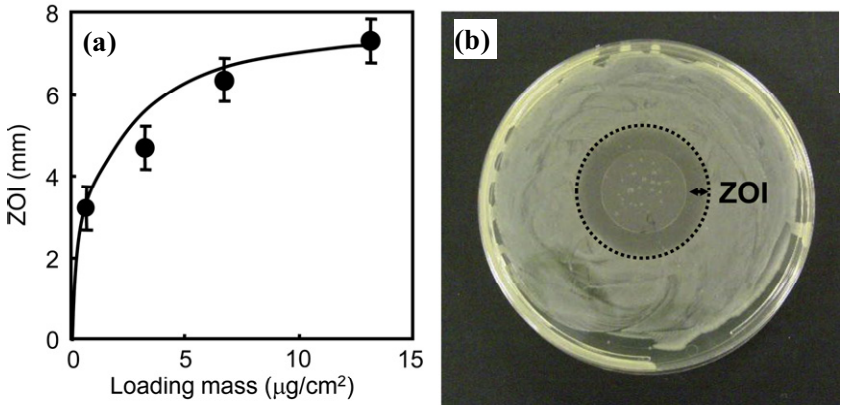

Fig. 6.4 (a) Antimicrobial property of different TC concentrations by the Kirby– Bauer (KB) test and (b) a representative image of the KB test indicating the zone of inhibition (ZOI).

In general, a clinically recommended dose of TC against *P. aeruginosa* as determined by the KB test is 94 μg/cm^2 (ZOI 3.5–7.0 mm), which was calculated from the datasheet approved by Clinical and Laboratory Standards Institute (CLSI) [4]. Hence, the TC-nanosheet could reduce the required amount of antibiotic by more than 15-fold compared to the clinically required dose.

4. Treatment of full-thickness burn with infection using antimicrobial loaded nanosheet

4.1. Preparation of burn-wound infection in mice and treatment with TC-nanosheet

In this experiment, male C57BL/6 mice weighing 22–25 g (8–9 weeks old, SLC, Shizuoka, Japan) were used. The mice were anesthetized by the intraperitoneal injection of sodium pentobarbital (50 mg/kg, Abbott Laboratories, North Chicago, IL) and their dorsal hair was clipped and depilated with a hair removal cream. The dorsal skin area (20% total body surface area) was then exposed to hot water (90 °C, 7 s) to induce a full-thickness burn-injury [5]. To prevent dehydration, all animals received intraperitoneal resuscitation of normal saline (1 mL).

After producing the full thickness burn-wound, a 100 μL aliquot of bacterial solution containing a known number of *P. aeruginosa* (1 x 10^8 CFU) was added topically to the wound area (Fig. 6.5 (a)). The wound infected area was then covered with TC-nanosheet/PVA material. The PVA supporting layer was subsequently dissolved by adding saline to leave the TC-nanosheet, where the nanosheet was tightly wrapped (TC (+), n = 10). As a control group, the wound area was also covered with a nanosheet that was not loaded with tetracycline (TC (-), n = 9). We also set up a burn-wound infection group without treatment with a nanosheet (sham group, n = 12) as well as a non-infection/non-treatment with nanosheet group (n = 9). To avoid cross-contamination, an occlusive dressing (Opsite Quick Roll, Smith and Nephew Co.) was applied immediately after treatment with the nanosheet. Opsite Quick Roll is a transparent and adhesive dressing that is used as a clinical secondary dressing to prevent contamination. Fig. 6.5 (b) and (c) shows the histological analysis of the dorsal skin before and after injury.

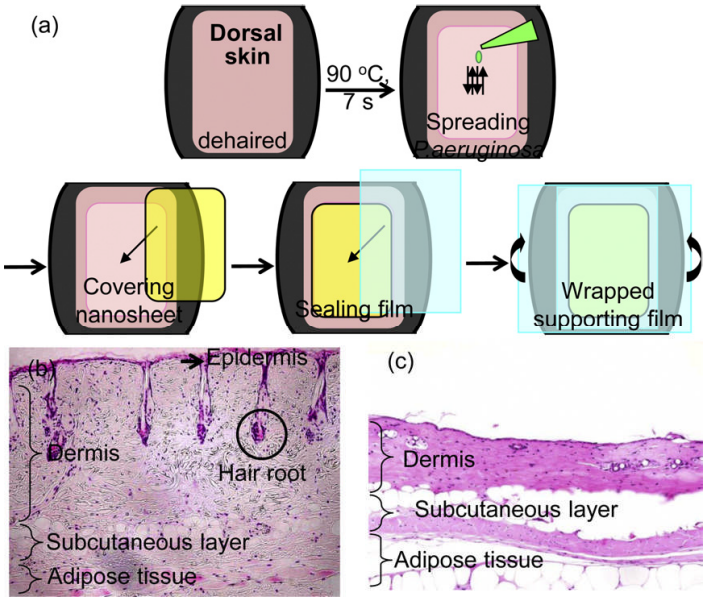

Fig. 6.5 (a) Preparation scheme for full-thickness burn-wound infection in a murine model. Histological images of murine dorsal skin (b) before and (c) after burn-injury.

The burn-wound lesion was covered with the TC-nanosheet after inoculation with *P. aeruginosa*. The TC-nanosheet on the wound area was transparent and thereby invisible under normal illumination (Fig. 6.6 (a)). Nonetheless, we were able to exploit the autofluorescence of TC to visualize the nanosheet as shown in Fig. 6.6 (b). Seven days after the operation, the TC-nanosheet was also observed under illuminating UV-light (Fig. 6.6 (c)). Therefore, the TC-nanosheet remained at the wound site for 7 days protected by Opsite Quick Roll as an occlusive secondary dressing.

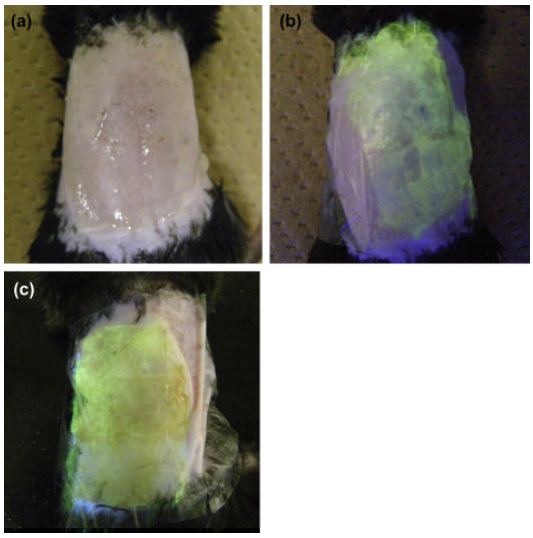

Fig. 6.6 Treatment of the full-thickness burn-wound infection with the TC-nanosheet. Macroscopic images of the murine dorsal skin, which was illuminated under (a) visible light and (b) by autofluoresence immediately after the operation, and (c) the same skin after 7 days.

The high transparency and fluorescent property of the TC-nanosheet facilitates monitoring of the burn-wound care management. It is noteworthy that visualization of the injured tissue may allow prompt and appropriate wound care in burn-injured patients. Hence, the transparency of the TC-nanosheet is an important property of this novel material, which has significant practical advantages over conventional wound-dressing materials.

We investigated the preparation of burn-wound infection in a murine model. Although all burn-injured mice without infection survived for 7 days, burn-injured mice with a wound infection showed only 40% survival over the same period of time (Fig. 6.7). Based on a comparison of the mice viability between sham and non-infection groups, dorsal infection with *P. aeruginosa* causes systemic inflammation, namely sepsis, in mice. The dorsal skin was fragile after burn injury, which presumably makes the damaged tissue susceptible to infection by *P. aeruginosa.* Therefore, we used this murine model to evaluate the antimicrobial properties of the TC-nanosheet *in vivo*.

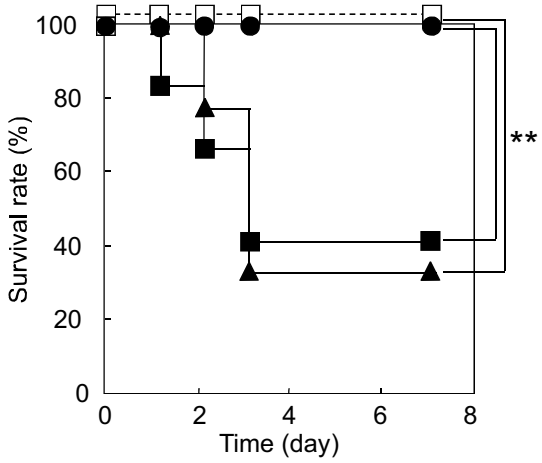

Fig. 6.7 Murine survival rate until 7 days after operation. (●, TC (+); ▲, TC (-); ■, sham; □, only full-thickness burn injury)

Although burn-wound infection significantly increased mouse mortality, the TC-nanosheet dramatically decreased the mortality of burn-wound infection (100% survival). By contrast, wound dressing using the TC (-) nanosheet (control) did not significantly improve survival rates after burn-wound infection compared to the sham group (i.e. >50% of mice were dead within 3 days).

4.2. Measurements of white blood cell (WBC) count

Blood samples were obtained from the retro-orbital plexus at 1, 2, 3 and 7 days after

injury and WBCs were counted using a PEC-170 hematology analyzer (Beckman Coulter, Hialeah, FL).

The mice receiving burn-wound infection showed higher WBC counts at 7 days after burn injury than those of mice without infection (Fig. 6.8). Mice treated with the TC-nanosheet showed a significantly lower WBC counts than other groups 7 days after injury/infection. The results of survival rate and WBC counts suggested that the TC-nanosheet successfully released TC, which acted as an antibacterial barrier against *P. aeruginosa*. Therefore, the TC-nanosheet inhibits bacterial infection by (i) directly suppressing bacterial activity and (ii) reducing subsequent systemic inflammation.

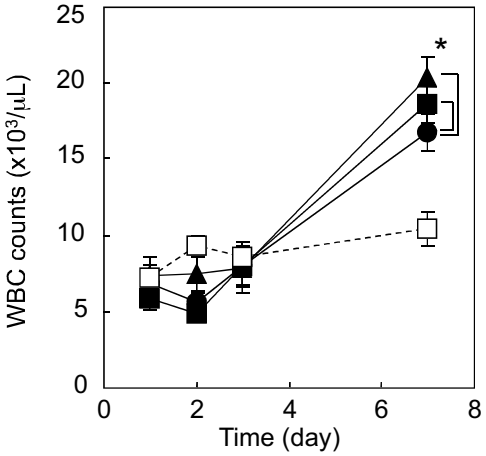

Fig. 6.8 WBC counts until 7 days after operation. (●, TC (+); ▲, TC (-); ■, sham; □, only full-thickness burn injury)

4.3. Viable bacterial count at the wound site

Three days after generating the burn and infection, the dorsal skin was taken and cut out at nine points by biopsy punch (5 mm diameter). The dorsal skins were homogenized in 1 ml of PBS. Ten-fold serial dilutions of the homogenized liver extract in PBS were spread on brain heart infusion agar plates and incubated at 37 °C in 5% CO_2 for 24 h. The number of colonies on the agar plates was then counted in order to determine the viable cell count.

Viable bacterial number at the wound site was

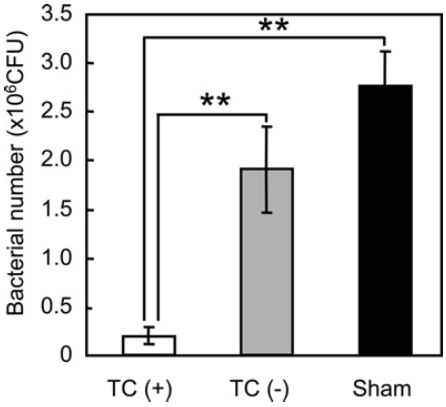

Fig. 6.9 Antimicrobial effects of the TC-nanosheet 3 days after the operation by counting bacterial numbers at the wound site (**P < 0.01). Error bars represent the standard deviation between experiments.

determined 3 days after the operation (Fig. 6.9). The TC-nanosheet suppressed the bacterial infection of *P. aeruginosa*. By contrast, there was no evidence of inhibition of bacterial growth at the wound area in the TC (-) and sham groups. Based on the number of viable bacteria at the wound site, it is clarified that the TC-nanosheet can prevent not only bacterial growth but also infection. Therefore, this result suggested that the TC-nanosheet could inhibit local inflammation.

4.4. Histological analysis

Dorsal skin and lung specimens were taken 3 days after injury, and then fixed with 10% neutral-buffered formalin. Histological sections were prepared from formalin-fixed, paraffin-embedded tissues stained using routine procedures with hematoxylin and eosin. The dorsal skin was also stained using routine procedures by a May–Grunwald Giemsa staining method. The numbers of inflammatory cells per field (877.12 μm x 655.95 μm) were counted in each image of the skin using Image J. The alveolar wall area ratio per field (877.12 μm x 655.95 μm) was measured in each image of lung using Image J. These analyses were performed in a blind fashion.

Histological analyses of the dorsal skin lesion and lung were undertaken 3 days after injury/infection. The dorsal skin lesion treated with the TC-nanosheet did not show severe inflammatory tissue response (Fig. 6.10 A(a)). In contrast, the dorsal skin lesion of the TC (-) group (Fig. 6.10 A(b)) as well as the sham group (Fig. 6.10 A(c)) displayed evident infiltration of leukocytes. May–Grunwald Giemsa staining was also performed and showed the same results as hematoxylin–eosin staining (Fig. 6.10 A(d)-(f)). Furthermore, when the number of inflammatory cells at the wound area was counted, the TC (+) group showed a significantly reduced number of inflammatory cells compared with both the TC (-) and sham

groups (Fig. 6.10 B).

Moreover, treatment with the TC-nanosheet evidently suppressed acute lung injury, which could be induced by burn injury as well as burn-associated infection (Fig. 6.11 A(a)). Both the sham group (Fig. 6.11 A(b)) and TC (-) group (Fig. 6.11 A(c)) showed severe acute lung injury with alveolar congestion, leukocyte infiltration in the septa and alveoli as well as interstitial edema. The alveolar wall area ratio of the TC (+) group was significantly lower than those of the TC (-) and sham groups (Fig. 6.11 B).

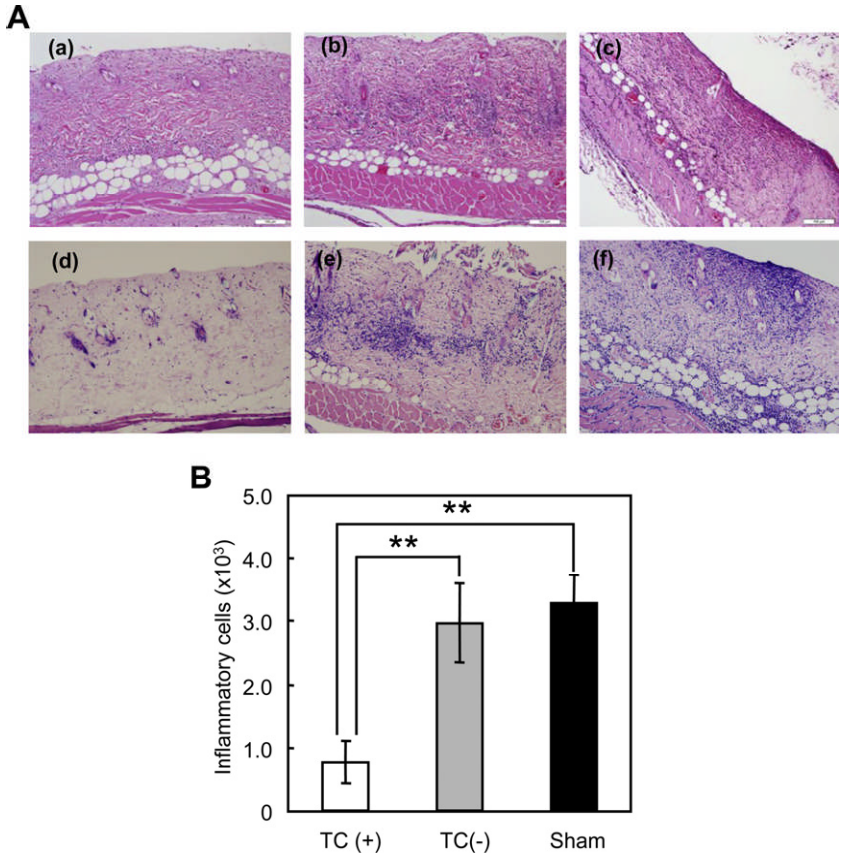

Fig. 6.10 (A) Histological analyses of dorsal skin stained with hematoxylin–eosin (top panels) and May–Grunwald Giemsa (bottom panels) after full-thickness burn-wound infection; treatment with (a, d) TC-nanosheet, (b, e) TC-unloaded nanosheet and (c, f) sham. (B) The number of inflammatory cells infiltrated into the injured skin counted by histological images (**P < 0.01)

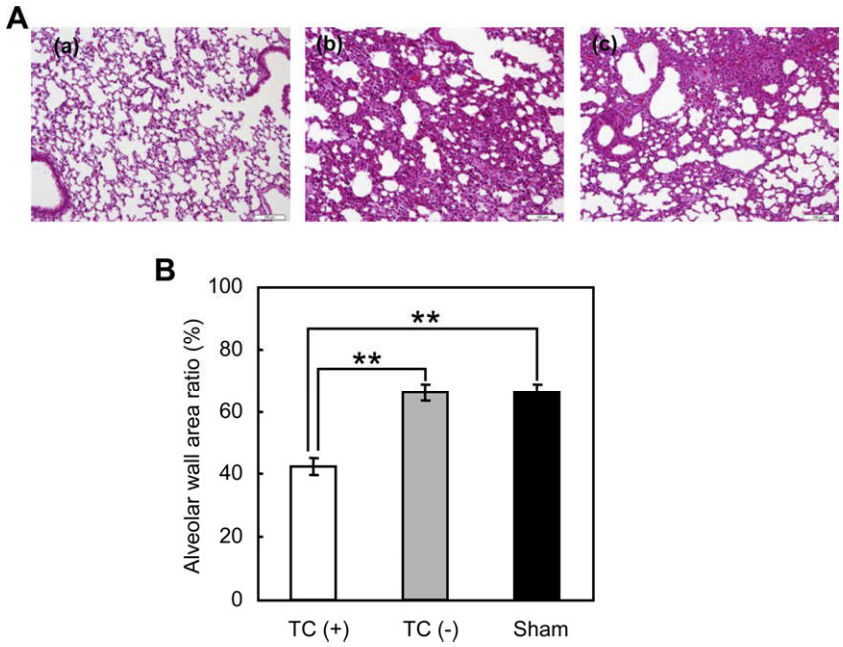

Fig. 6.11 (A) Histological analysis of lung after full-thickness burn-wound infection; treatment with (a, d) TC-nanosheet, (b, e) TC-unloaded nanosheet and (c, f) sham. (B) Alveolar wall area ratio measured by histological images (**P < 0.01).

Histological analysis of dorsal skin showed that local wound infection by *P. aeruginosa* was suppressed by the TC-nanosheet. In contrast, the TC (-) and sham groups did not improve burn-wound infection. These findings indicated that the TC-nanosheet effectively prevented bacterial infection in the burn-wound lesion. Moreover, the reduction in the number of inflammatory cells at the site of injury showed that the TC-nanosheet can prevent local inflammation. Furthermore, pathological findings, which involved measuring alveolar wall area ratios, indicated a reduction in systemic inflammation in the TC-nanosheet group. These results suggest that protection by the TC-nanosheet suppressed not only local tissue damage (e.g. skin) but also remote organ injury (e.g. lung). Hence, the TC-nanosheet effectively prevented a systemic inflammatory response as well as local inflammation after burn-wound infection.

4.5. Viable bacterial count in the liver

Three days after generating the burn and infection, the liver was aseptically removed

from the mice under deep anesthesia and homogenized in 1 ml of PBS. Ten-fold serial dilutions of homogenized liver extract in PBS were spread on brain heart infusion agar plates and incubated at 37 °C in 5% CO_2 for 24 h. The number of viable bacteria was then counted according to the observed colonies on the agar plates.

Mice treated with the TC-nanosheet displayed a significant reduction (>20-fold) in bacterial growth in the liver compared with the TC (-) and sham groups (Fig. 6.11).

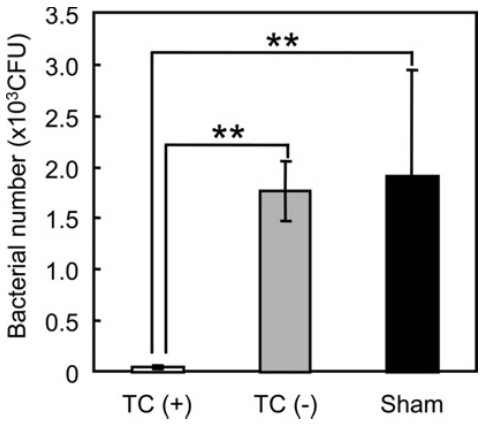

Fig. 6.11 Antimicrobial effects of the TC-nanosheet 3 days after the operation by analyzing bacterial numbers in liver **P < 0.01). Error bars represent the standard deviation between experiments.

Elimination of bacteria from the systemic circulation is generally attributed to phagocytosis by tissue macrophages. Approximately 80% of tissue macrophages reside in the liver as Kupffer cells. Thus, bacterial clearance/elimination in the liver is a crucial problem for the host. We have demonstrated that severe burn-injury induces immunosuppression and thereby attenuates bacterial clearance in the liver, thus resulting in high morbidity and mortality of post-burn infections [6,7]. Moreover, it is generally known that burn-injury disrupts barrier function of gut. The injury causes dissemination of bacteria from the intestinal tract, and allows bacterial translocation (BT) to the liver, mesenteric lymph nodes and spleen [8,9]. The seriousness of BT is determined by the severity of the burn injury [10]. Measurement of bacterial count in the liver may elucidate the extent of bacterial elimination activity in this organ of burn-injured mice. The result of 3.6 suggested that treatment with the TC-nanosheet pre- served the activity of bacterial elimination in the liver. Therefore, the TC-nanosheet may suppress not only bloodstream infection (septicemia) spreading from the site of a burn-wound infection but also burn-associated BT in mice. We previously reported that bacteria could penetrate

nanosheets not loaded with antibiotic [2]. In this respect, loading the nanosheet with an antibiotic is a critical factor in their application as a novel wound-dressing and protective material.

The advantages of TC-nanosheet compared with other wound dressings, such as Acticoat® and Aquacell®, are high flexibility, high adhesive strength and high transparency. In this paper, the TC- nanosheet was used to cover the dorsal skin, which is moderately flat. Thus, the nanosheet would be expected to give similar results to those of other dressing materials. However, the nanosheet can also be applied to more complex shapes, such as a fingertip. In these circumstances, the nanosheet can cover the wound area more easily than other dressing materials due to its inherent flexibility and considerable adhesive strength. Furthermore, the TC-nanosheet improves the viability of the wound site due to its high level of transparency. With other, less transparent wound dressings, it is difficult to manage the wound site. Conventional dressings need to be changed on a daily basis in order to monitor whether the wound site has become infected. However, this procedure increases the risk of bacterial infection. By contrast, our TC-nanosheet diminishes the chances of infection because the wound site can be observed without opening the transparent occlusive dressing for at least one week. The nanosheet alone can- not maintain a suitable moisture level at the wound site as well as protect the wound. However, a combination of TC-nanosheet with Opsite Quick Roll protected the wound site mechanically and maintained the moisture level in addition to effectively preventing bacterial infection.

5. Summary

We investigated the antimicrobial effect of a TC-nanosheet as a wound-protecting

material for burn-wound infection in a murine model. The TC-nanosheet can be easily fixed on the burn-injured skin without chemical glue. Moreover, the transparent properties of the dressing material allow observation of the wound care management until tissue grafting can be performed. The TC-nanosheet has a potent antibacterial activity, thereby inhibiting burn-wound infection. We conclude that the TC-nanosheet is a promising therapeutic tool for burn-wound management in severely burn-injured patients.

References

88) N. Brusselaers, A. Pirayesh, H. Hoeksema, C. D. Richters, J. Verbelen, H. Beele, *et al., J. Trauma*, **68**, 490 (2010).

89) T. Fujie, A. Saito, K. Kinoshita, H. Miyazaki, S. Ohtsubo, D. Saitoh, S. Takeoka, *Biomaterials*, **31**, 6269 (2010).

90) B. S. Speer, N. B. Shoemaer, A. A. Salyers, *Clin. Microbiol. Rev.,* **5**, 387 (1992).

91) Clinical and Laboratory Standards Institute. Performance standard for anti-microbial susceptibility testing. Document M100–S15. Wayne, PA: CLSI (2005).

92) J. Patenaude, M. D'Elia, C. Hamelin, D. Garrel, J. Bernier, *J. Leukoc. Biol.,* **77**, 141 (2005).

93) M. Kinoshita, N. Shinomiya, S. Ono, H. Tsujimoto, T. Kawabata, A. Matsumoto, *et al., J. Immunol.* **177**, 4627 (2006).

94) M. Kinoshita, S. Seki, N. Shiomiya, H. Hiraide, *Ann. Surg.* **24**, 313 (2004).

95) R. D. Berg, W. E. Owens, *Infect. Immun.,* **25**, 820 (1979).

96) D. H. Chung, D. N. Herndon, *Crit. Care. Med.,* **32**, 1803 (2004).

97) Gianotti L, Alexander JW, Pyles T, James L, Babcock GF. J Burn Care Rehabil 1993;14:336–42

Chapter 6.

Conclusions and future prospects

1. Conclusions

In this thesis, the author described the medical efficiency of the polymer nanosheets as new type wound dressing material. The notable characteristics obtained from the respective study are summarized below. The author convinced that the nanosheet is revolutionary development of wound dressing material that can on-demand wound observation under the surgery and after operation.

1. The anti-adhesive efficiency of PLA nanosheet was investigated. The nanosheet can attach onto the injured organ directly. Conventional materials such as Seprafilm® were less adhesiveness and the directly sealing is difficult because their low flexibility. We investigate the new methodology and concept of anti-adhesive materisl (chapter 3)

2. The haemostatic efficiency of LbL nanosheet was investigated. Moreover, multi-overlapping therapy that is methodology of improvement of nanosheet. The methodology was effectively stopped the massive haemorrhage from IVC. Additionally, the operation time was more dramatically shortened than conventional suturing. (chapter 4)

3. The fragmentation of PLLA nanosheet was succeeded. To fragment the nanosheet, the nanosheet dispersed in water. The fragmented nanosheet can reconstruct onto various surfaces. The reconstructed nanosheet can protect the bacterial infection until 3 days. (chapter 5)

4. The new application of antimicrobial loaded nanosheet was performed. The nanosheet can reduce the bacterial infection of full-thickness burn. The nanosheet can inhibit not only local but also systemic inflammation. (chapter 6)

2. Future prospects

The author summarized nanosheet application for medical. These applications are more revolutionary than conventional wound dressing materials. In the future development, the nanosheet will functionalize although the nanosheet has high range of application. The author described the future prospects of the new drug delivery tool.

In this thesis, the author proposed two types of functionalization that is fragmentation and drug loading. Therefore, the author proposes the “drug loaded fragmented nanosheet” The strong point of fragmented nanosheet is easy to cover the complex surfaces. If some drugs can be loaded into fragmented nanosheet, the new drug delivery material can cover the complex wound. Moreover, fragmented nanosheet will be sprayed to surface due to their small size. For representative example, pressure sore is complex wound. The drug loaded fragmented nanosheet such as loading the growth factor will be sprayed on the pressure sore easily. This approach will be a new treatment methodology.

Academic Achievement

(List of Pubrication)

1) Hagisawa K*, Saito A*, Kinoshita M, Fujie T, Otani N, Shono S, Park, S YK. Takeoka S (*equority contributed) "Effective control of massive venous bleeding by "multi-overlapping therapy" using polysaccharide nanosheets in a rabbit inferior vena cava injury model" *J. Vasc. Surg.: Venous Lymphatic Disorders*, **1**, 289 (2013).

2) Fujie, T, Kawamoto, Y, Haniuda, H, Saito, A, Kabata, K, Honda, Y, Ohmori, E, Asahi, T, Takeoka, S "Selective Molecular Permeability Induced by Glass Transition Dynamics of Semicrystalline Polymer Ultrathin Films" *Macromolecules*, **46**, 395 (2013).

3) Aoki S, Kinoshita M, Miyazaki H, Saito A, Fujie T, Iwaya K, Takeoka S, Saitoh D. "Application of poly-L-lactic Acid nanosheet as a material for wound dressing" *Plast. Reconstr. Surg.*, **131**, 236 (2013).

4) Otani N, Kinoshita M, Fujie T, Saito A, Takeoka S, Saitoh D, Hagisawa K, Nawashiro H, Shima K "Novel therapeutic use of polysaccharide nanosheets for arachnoid plasty and enhancement of venous tensile strength in rat microneurosurgery" *J. Clin. Neurosci.,* **20**, 301 (2013).

5) Okamura Y, Kabata K, Kinoshita M, Miyazaki H, Saito A, Fujie T, Ohtsubo S, Saitoh D, Takeoka S "Fragmentation of Poly(lactic acid) Nanosheets and Patchwork Treatment for Burn Wounds" *Adv. Mater*., **25**, 545 (2013).

6) Miyazaki H, Kinoshita M, Saito A, Fujie T, Kabata K, Hara E, Ono S, Takeoka S, Saitoh D "An ultrathin poly(L-lactic acid) nanosheet as a burn wound dressing for protection against bacterial infection." *Wound Repair Regen.*, **20**, 573 (2012).

7) Saito A, Miyazaki H, Fujie T, Kinoshita M, Ohtsubo S, Saitoh D, Takeoka S, "Therapeutic efficacy of an antibiotic-loaded nanosheet in a murine burn-wound infection model." *Acta Biomater.*, **8**, 2932 (2012).

8) Fujino K, Kinoshita M, Saito A, Yano H, Nishikawa K, Fujie T, Iwaya K, Kakihara M, Takeoka S, Saitoh D, Tanaka Y "Novel technique of overlaying a poly-l-lactic acid nanosheet for adhesion prophylaxis and fixation of intraperitoneal onlay polypropylene mesh in a rabbit model." *Surg. Endosc.*, **25**, 3428 (2011).

9) Taccola S, Desii A, Pensabene V, Fujie T, Saito A, Takeoka S, Dario P, Menciassi A, Mattoli V, Free-Standing Poly(l-lactic acid) Nanofilms Loaded with Superparamagnetic Nanoparticles." *Langmuir*, 27, 5589 (2011)

(Review)

1) 齋藤晃広, 武岡真司 "高分子ナノシートの物性と医療展開" *未来材料*, **11**, 24 89 (2011).

2) 藤枝俊宣, 齋藤晃広, 武岡真司 “医療応用に向けた高分子超薄膜の新展開” *表面*, **48**, 211 (2011).

(International Symposium)

1) Saito A, Miyazaki H, Fujie T, Ohtsubo S, Kinoshita M, Saitoh D, Takeoka S “Evaluation of Therapeutic Efficiency of Antibiotic-Loaded Nanosheet in a Murine Burn-Wound Infection Model” 2nd International Conference on Biomaterials Science in Tsukuba, Tsukuba, 2013.3

2) Saito A, Miyazaki H, Fujie T, Ohtsubo S, Kinoshita M, Saitoh D, Takeoka S “Therapuitic effects of tetracycline-loaded nanosheet for a deep burn-wound infection model” 243rd ACS National Meeting, San Diego, USA, 2012.3

3) Saito A, Takeoka S “Antibacterial efficiency of silver nanoparticle-loaded nanosheet” Japan-India Joint Workshop on “Biomedical Research”, Tokyo, 2012.2

4) Saito A, Takeoka S “Antibacterial effciency of silver nanoparticle loaded nanosheet” German-Japanese Joint Symopsium for Diamond Researchers on Sustainable Life Science Innovation and Biomedical Research, Bonn, German, 2011.12

5) Saito A, Fujie T, Miyazaki H, Kinoshita M, Saitoh D, Takeoka S “Fabrication and evaluation of silver-nanoparticle loaded nanosheet” The 6th Global COE international Symposium, Tokyo, 2011.12

6) Saito A, Fujie T, Miyazaki H, Kinoshita M, Saitoh D, Takeoka S “Fabrication and evaluation of silver-nanoparticle loaded nanosheet” The 3rd NIMS-Waseda International Symposium, Tokyo, 2011.11

7) Saito A, Miyazaki H, Fujie T, Kinoshita M, Saitoh D, Takeoka S “Antimicrobial Effects of Tetracycline Loaded Nanosheets for Deep Burn Infectious Model Mice” 5th GCOE International Symposium, Tokyo, 2011.1

8) Saito A, Miyazaki H, Fujie T, Kinoshita M, Saitoh D, Takeoka S “Antimicrobial Effects of Tetracycline Loaded Nanosheets for Deep Burn Infectious Model Mice” 2nd NIMS(MANA)-Waseda International Symposium, Tsukuba, 2010.12

他連名 7 件

(Domestic Symposium)

1) 齋藤 晃広, 武岡 真司 ”高分子ナノシートによる下大静脈止血” 新宿バイオマテリアルの会, 新宿, 2013.1

2) 齋藤 晃広, 萩沢 康介, 小川 大輔, 木下 学, 朴 栄光, 梅津 光生, 武岡 真司 “高分子ナノシートを用いた静脈止血材としての応用” 日本バイオマテリアル学会シンポジウム 2013, 仙台, 2012.11

3) Saito A, Ito K, Fujie T, Takeoka S “Antimicrobial efficiency of silver nanoparticle-loaded nanosheet”第 61 回高分子討論会, 名古屋, 2012.9

4) 齋藤 晃広, 木下 学, 宮崎 裕美, 藤枝 俊宣, 齋藤 大蔵, 武岡 真司 “抗生物質担持ナノシートを用いたIII度熱傷治療への有用性” 第 112 回日本外科学会定期学術集会, 幕張, 2012.4

5) 齋藤 晃広, 宮崎 裕美, 藤枝 俊宣, 木下 学, 齋藤 大蔵, 武岡 真司 “抗生物質担持ナノシートのIII度熱傷・感染に対する創傷保護材としての有用性” 第60回高分子学会年次大会, 大阪, 2011.5

6) 齋藤 晃広, 宮崎 裕美, 藤枝 俊宣, 木下 学, 齋藤 大蔵, 武岡 真司 “薬剤担持ナノシートのIII度熱傷･感染に対する創傷保護能評価” 第32回日本バイオマテリアル学会大会, 広島, 2010.11

他連名 10 件

(Patent)

1) 阿部公司，八巻悟史，武岡永里子，武岡真司，藤枝俊宣，下野浩貴，齋藤晃広（株式会社資生堂、ナノシータ株式会社），粉末担持薄膜，国内，特許公開 2013-1661，2013.1.7

2) 宮地計二，小林義典，甘利昌彦，武岡真司，藤枝俊宣，齋藤晃広，張宏，大坪真也（甘利昌彦、学校法人早稲田大学），高分子超薄膜の製造方法及び高分子超薄膜の製造装置，国内，特許公開 2012-236125，2012.12.6

3) 武岡真司，柏木賢治，藤枝俊宣，齋藤晃広（武岡真司、国立大学法人山梨大学），医薬製剤，国際，PCT/JP2012/057519，2012.3.23

(Press Release)

1) 萩沢 康介, 齋藤 晃広, 木下 学, 藤枝 俊宣, 大谷 直樹, 庄野 聡, 朴 栄光, 武岡真司 “静脈止血剤としてのナノ絆創膏の開発” 日本経済新聞, 日経産業新聞, 科学新聞, 毎日新聞, 日刊工業新聞, 化学工業日報 2013 年 5 月

Acknowledgements

The presented thesis is the collection of the author's studies, which have been carried out under the direction of Prof. Shinji Takeoka at the Department of Life Science and Medical Bioscience, Waseda University during 2011-2013. The author expresses the greatest acknowledgement to Prof. Shinji Takeokafor his valuable suggestions, helpful discussions, and continuous encouragement throughout this work. The author also expresses his sincere gratitude to Prof. Yasuo Ikeda and Prof. Nobuhito Goda for the efforts as members of the judging committee for the doctorial thesis.

The author also expresses special thanks to the members of National Defense Medical College. In particular, grateful acknowledgement is made to Prof. Dr. Daizoh Saitoh, Assoc. Prof. Dr. Manabu Kinoshita, Dr. Hiromi Miyazaki, Dr. Kosuke Hagisawa, Dr. Akinari Hinoki for their valuable suggestions.

The author gratefully acknowledges to his mentor from bachelor to doctorial Course, Dr. Toshinori Fujie for discussions with full passion not only on his research but also on his way of life. His attitude towards science always inspired the author.

The author gratefully acknowledges to Mr. Shinya Ohtsubo to his mentor about collaborative research of nanosheet group. The author can gather many experiences.

The author expresses his acknowledgement to Dr. Yosuke Okamura, Dr.Satoshi Arai, Dr. Daisuke Niwa, Dr. Atsushi Murata, Dr. Satya Ranjan Sarker, Dr. Hong Zhang, Miss. Thienshu Li.

The author expresses the remarkable thanks to the member of Nanosheet group, Mr. Yoshihito Fukui, Mr. Koki Kabata, Mr. Sho Furutate, Mr. Hiroki Haniuda, Mr. Masatsugu Koide, Miss Yuko Kawamoto, Mr. Keisuke Ito, Mr. Gen Noguchi Mr. Shoichiro Suzuki, Miss. Mao Fujii, Mr. Yuya Ishizuka, Mr. Katsuhiro Sato. Without their tremendous efforts and powers, the author would not accomplish his work.

All members in the Laboratory of Biomolecular Assembly and the Laboratory of Polymer Chemistry offered kind assistance for which the author would like to thank deeply. The author acknowledges to Global COE Program "Practical Chemical Wisdom".

Finally, the author expresses his deepest gratitude to his family, Mr. Hajime Saito, Mrs. Noriko Saito for their affectionate contributions.

July, 2013
Akihiro Saito